IEEE Access
Multidisciplinary | Rapid Review | Open Access Journal

Received 25 March 2022, accepted 8 June 2022, date of publication 22 June 2022, date of current version 11 July 2022.

Digital Object Identifier 10.1109/ACCESS.2022.3185240

Sequential Fusion Based Approach for Estimating Range Gate Pull-Off Parameter in a Networked Radar System: An ECCM Algorithm

PURUSHOTTAMA LINGADEVARU, (Member, IEEE), BETHI PARDHASARADHI, (Member, IEEE), AND PATHIPATI SRIHARI, (Senior Member, IEEE)
Department of Electronics and Communication Engineering, National Institute of Technology Karnataka, Surathkal 575025, India

Corresponding author: Pathipati Srihari (srihari@nitk.edu.in)

ABSTRACT Networked radar is an emerging and effective alternative to traditional radar systems to provide improved performance by fusing information from multiple radars. Further, networked radar systems (NRS) have found numerous deployments in military and civilian infrastructures in recent years. Electronic countermeasures (ECM) like jamming, Range Gate Pull-Off (RGPO), and Velocity Gate Pull-Off (VGPO) generally pose a high risk to the radar systems by injecting intentional interference. This paper proposes networked radar to detect the RGPO ECM attack and estimate the range gate deception parameter of the deceived local track in an NRS. Each radar comprises a local tracker to provide the local estimates (updated state and updated covariance), and these estimates are then sent to the fusion node. Thereafter, a track-to-track association (T2TA) is formulated at the fusion node to detect the deceived tracks using all the available local tracks. For the deceived track, the pseudo-measurements are created using the inverse Kalman filter-based tracklets. All the local tracks except deceived track are compensated and sequentially fused to create a reference measurement. After that, the deception parameter of the deceived track is estimated by using pseudo-measurement and the reference measurement by employing the recursive least square estimator (RLSE). In addition, the proposed algorithm is analyzed for single and multiple RGPO based ECM scenarios. Further, the Cramer Rao Lower Bound (CRLB) for the proposed methodology is derived. The results are quantified with a Position Root Mean Square Error (PRMSE), CRLB, innovation test, normalized estimation error squared (NEES) test, and confidence interval. The simulation results demonstrate that the proposed estimation technique provides good performance in the presence of all the local tracks are being attacked by RGPO ECM. Besides, it is evident from the results that estimator efficiency is falling below the 5% tail probability of the chi-square distribution.

INDEX TERMS Cramer-Rao lower bound, electronic counter countermeasure, networked radar, range gate pull-off, sequential fusion, tracklets.

I. INTRODUCTION

Networked radar has been very prominent in recent years for the abundant resources it can use, specifically in target tracking applications. A networked radar system (NRS) connects several heterogeneous radar systems geographically located at different locations to a fusion center to jointly detect and monitor targets in a large surveillance region [1]. Since an NRS can significantly boost the precision of detection and monitoring targets, it finds a wide range of applications, such as air traffic control, military intelligence, and autonomous vehicles etc. Further, radar networks are widely adopted in civilian and military infrastructures, ECM attacks may pose a significant challenge to national security and to the economy [2].

Electronic countermeasure (ECM) techniques have become increasingly important in modern warfare, with rapid advances in electronic technology and military intelligence. Various ECM techniques have been proposed in the literature, namely noise jamming, Stand-Off Jamming (SOJ), Self Screening Jamming (SSJ), RGPO, and VGPO [3]. Noise jamming is an ECM in which the enemy radar transmits

The associate editor coordinating the review of this manuscript and approving it for publication was Geng-Ming Jiang.

This work is licensed under a Creative Commons Attribution 4.0 License. For more information, see https://creativecommons.org/licenses/by/4.0/

a noise signal with increased strength at the radar's operating frequency, such that the signature from the target is completely melded with the interference. On the other hand, in the SOJ technique, the high-power jamming signal is transmitted from the enemy radar at a larger distance than the maximum range at which the targeted radar can detect the targets. In SSJ, jamming equipment is carried out for self-protection, and efficient jamming geometry between victim radar and jammer is always maintained. Deception jamming techniques like RGPO and VGPO are the most productive of all the ECM techniques that generate fake targets in order to deceive target tracking systems [4]. RGPO is a sort of ECM that intercepts radar signals and retransmits a deception signal with a progressive time delay, pulling the range gate of the radar target tracker further away from the actual target over time [5]. On the other hand, VGPO is employed by injecting a frequency-shifted replica of the received radar signal; the frequency of the false return is slowly altered to interfere with the true Doppler shift [6]. Digital radio frequency memory (DRFM) devices are generally used to store and regenerate captured radar signals to confuse hostile radars [7]. In addition, because of advances in computing capability and hardware architecture, the DRFM can simultaneously process multiple captured signals, allowing a modern repeater to deploy deception jamming on multiple-radar devices [7]. The DRFM is utilized to gradually delay the deception signal, thereby ''walking'' the range gate away from the true target. The RGPO deception jamming produced by the DRFM system is highly coherent to the radar transmitted signal, which makes the detection of the deception jamming difficult [8].

Electronic Counter Countermeasure (ECCM) are broadly classified into signal analysis and target tracking. In signal processing, most radar systems are provided with ECCM capabilities to combat deception jamming in recent years. The ECCM techniques such as pulse diversity, polarization character, motion function, DRFM quantization error, and target detection system in the presence of interference ensure that no single radar is tricked [7], [9]–[13]. In [14], an efficient ECCM approach for countering the very high-power ECM using an orthogonal frequency division multiplexing (OFDM) radar is presented and analyzed. Here, the phase codes of the sub-carriers belonging to the OFDM pulses are tuned to limit the jamming strength to suppress range deception and combined range-velocity deception jamming [14].

Most of the sensors may not be aware of the ECM techniques; however, they are resolved using efficient target tracking. The effect of RGPO on radar target tracking with benchmark targets is studied in [15] and [16]. In particular, controlling the beam pointing of phased array radar for benchmark target tracking problems in the existence of RGPO and false alarms is investigated in [15], [16]. The impacts of target amplitude variations, beam shape, missed detections, false alarms, finite resolution, target motions, and track loss were all included in the test-bed simulation described in [15]. Further, in [17] the solution for the second Benchmark problem of tracking a maneuvering target in the existence of RGPO using variable state dimension Kalman filter is presented. Authors in [17], have deployed adaptive waveform selection and dwell revisit time selection methods and track filter coasting for handling the uncertainties introduced by false alarms, missed detection, maneuvers, and RGPO. Further, for tracking highly maneuvering targets, a comprehensive framework is presented in [3] in the presence of false alarms, SOJ, and RGPO. Mainly, the algorithms for track generation and maintenance, adaptive target revisit interval selection, waveform selection, and detection threshold; and neutralizing ECM approaches were discussed in depth in [3]. The interacting multiple model (IMM) estimator in combination with the probabilistic data association (PDA) technique is utilized for tracking the targets in [3]. Additionally, authors in [18] have suggested the solution to the benchmark target tracking, which addresses the efficient resource allocation in the presence of ECM. The resource allocation problem is solved using interacting multiple model/multiple hypothesis tracking (IMM/MHT) tracker along with target tracking [18].

In [19], to counter RGPO and Range Gate Pull-In (RGPI) jamming, an ECCM approach based on loss of balance in the range tracking loop is presented and analyzed. Further, using adaptively updated bias weight in every range tracking interval according to the error signal, which balances the energy of the early and late gates concerning the target and continues to track the target with insignificant track loss is presented in [19]. Furthermore, memory tracking and narrow gate monitoring were used to propose and assess a novel ECCM approach against deception jamming in [20]. In addition, authors in [20] have concluded that the proposed method provides significant efficacy while countering all types of RGPO. In [21], the spatial filtering technique using trilinear decomposition to overcome the effect of deception jamming is presented and analyzed. Further, authors in [22] have proposed a composite approach to estimate the location of the target and deception range for distinguishing between false targets and true targets. The data fusion-based approaches are proposed to distinguish false targets using data correlation algorithms and local radar measurements (range, angle, and Doppler information). On the other hand, signal fusion-based techniques explore the ECCM abilities of multiple-radar systems by utilizing amplitude and phase information of the target echoes to provide efficient countermeasures [23]. The most generic and systematic approach for mitigating the effect of RGPO on target tracking is Decomposition and Fusion (DF) where, the deception measurements have virtually the same angles like that of true measurements [24], [25]. The fundamental steps involved in the DF technique are decomposition of validated measurements using hypothesis testing, track filtering for range deception measurements, conventional filtering, and performing a fusion of these estimates.

Considering the above review of the literature, most of the existing contributions have been addressed the effect of RGPO in either signal or target tracking perspective. Here,

we have assumed two cases. Case-1: Inadequate signal processing based ECCM techniques have been deployed and yet few RGPO ECM corrupted measurements are arriving for data processing (target tracking) and a simple target tracking algorithm is working. Case-2: There are no signal processing based ECCM techniques have been deployed and measurements are completely corrupted by RGPO ECM and a simple target tracking algorithm is working. Hence, in either case the tracks being reported by the tracker are falsified due to RGPO ECM. Further, there are insignificant research works that focus on countermeasures to ECM in a networked radar from a target tracking and fusion perspective. Hence, in this paper, we consider an NRS and all the radars contain a local tracker to estimate the updated state and covariance of targets. These local tracks are available at the fusion center and performed a T2TA to detect the RGPO ECM attack. It is noted that the detection lone is inadequate unless the mitigation measures are provided. Hence, this motivated us to carry out this investigation to estimate the deception parameter of each local track. To construct equivalent measurements of the deceived track, one requires a Kalman gain, which is unavailable from the local tracker. Hence, a tracklet based framework is considered to re-create a Kalman gain followed by pseudo-measurements and pseudo-measurement covariance. Similarly, all the available local tracks except the deceived track are compensated with the estimated deception parameter and generated a reference measurement using a sequential fusion algorithm. The pseudo-measurements and reference measurement are then used in the recursive least squares framework to estimate the deception parameter of the deceived track. The following are the major contributions of the paper are:

- We propose to estimate the deception parameter at the fusion center in an NRS to provide an efficient countermeasure to the RGPO ECM technique.
- We employed inverse Kalman filter-based tracklets to construct the pseudo-measurement from the available updated state and covariance.
- The reference measurement is created by compensation and sequential fusion of all the available tracks except the deceived track.
- The RLSE framework is used to estimate the deception parameter of the deceived track by using pseudo-measurement and reference measurement. Further, innovation test, confidence interval, and normalized estimation error squared (NEES) test to validate the effectiveness of the proposed deception parameter estimation algorithm.

The paper is structurally organized as follows: Section II outlines the problem formulation, section III describes the distributed target tracking using local trackers and track to track association. Further, section IV presents the proposed deception parameter estimation algorithm. In addition, section V proposes various tests like innovation test, NEES test and confidence interval test to validate the proposed method. Besides, section VI presents the results and discussions and the paper is concluded with the concluding remarks and future work in section VII.

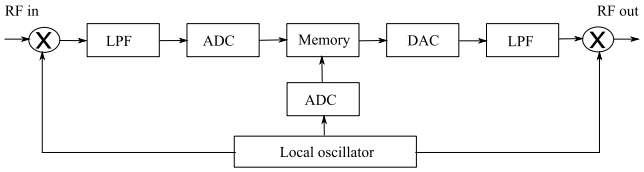

FIGURE 1. DFRM block diagram.

II. PROBLEM FORMULATION

A. DFRM RGPO MODEL

DRFM systems digitize the received signals and store them into the memory. Thereafter, alter the stored signals and re-transmit them towards the radar to create an illusion that true target is present. DRFM consists of receivers, analog-to-digital converters (ADC), electronic attack (EA) control system, digital-to-analog Converters (DAC), and transmitters [26]. The basic structure of a traditional DRFM is depicted in Fig. 1.

For deceiving a radar using a DRFM system the radar signals are captured and stored in the memory. These stored signals can be used to synthesize single or multiple false targets to intentionally misguide the radar. The input radio frequency (RF in) signal is often down-converted in frequency before being sampled with a high-speed ADC in a DRFM system. The stored samples are first altered in terms of amplitude, frequency, and phase, then processed by a DAC, up-converted, and sent back (RF out) to the victim radar so as to generate the false targets [27]. Further, a DRFM system can modify the signature of the target by altering its apparent radar cross section, range, velocity, and angle before re-transmitting the signal. There are several key DRFM based ECM techniques: 1. Generation of multiple false targets, 2. RGPO and VGPO, 3. Inverse gain and 4. Bin masking. Among these techniques, the deception jamming performed in range domain, to deceive the radar is known as RGPO. Accordingly, in this paper, we have considered countering RGPO ECM at measurement level processing using the sequential fusion based algorithm in a networked radar framework. The established RGPO measurement model presented in [28] and is represented as,

$$r_d(k) = \begin{cases} r(k), & t_k \leq t_0 + T_{ca} \\ r(k) + \Delta r(k), & t_k > t_0 + T_{ca} \end{cases} \quad (1)$$

where, $r_d(k)$ is the deceived false range of the target from the radar, $r(k)$ is the actual range, and $\Delta r(k) = \frac{c\Delta t_k}{2}$ is the deviation in the range owing to RGPO ECM. Here, Δt_k is the time delay due to ECM delay line as presented in [28]. Further, t_0 is the start time of the range deception, c is the speed of light and, T_{ca} represents the length of the false target evolving time.

B. RGPO IN NETWORKED RADAR SYSTEM

Consider a surveillance area being monitoring by NRS, where the number of radars is greater than two. Assume that all

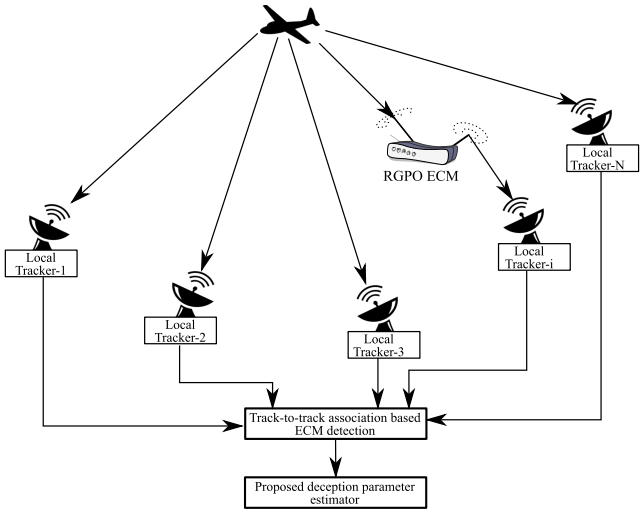

FIGURE 2. Scenario illustrating networked radars, RGPO jammer, and target.

the radars are synchronized and provides the measurements pertaining to the targets. The measurement space of the radar is range and azimuth. A deception jammer is placed in the same surveillance region and sending spurious signals to mislead either one or more radars in the given surveillance. The measurement at the one or more radars are corrupted by range gate pull off (RGPO) ECM technique. The scenario of NRS in which one of the radar is deceived by a single RGPO jammer as shown in Fig. 2. In the first case, a single radar sensor as shown in Fig. 2, is assumed to be affected by the RGPO jamming and results in deceived track as shown in Fig. 3a. Whereas, in the second case, multiple radar sensors are considered to be affected by ECM and leads to multiple deceived tracks as shown in Fig. 3b.

The target state model is represented as,

$$\mathbf{x}(k+1) = \mathbf{F}\mathbf{x}(k) + \Gamma_x \mathbf{v}(k), \tag{2}$$

where $\mathbf{x}(k)$ is m_x dimensional state vector consisting of position and velocity of the target at the discrete time instant k. $\mathbf{F}$ is the state transition matrix which follows constant velocity (CV), constant turn (CT), and constant acceleration (CA) depending on the state dynamics. Γ_x is noise gain matrix [29] and $\mathbf{v}(k)$ is the process noise that follows Gaussian PDF with covariance,

$$\mathbf{Q}_x = E[\mathbf{v}(k)\mathbf{v}(k)^T]. \tag{3}$$

Here $E[.]$ and $[.]^T$ represents the expectation and transposition operator respectively.

The measurement model without the influence of ECM is given by,

$$\mathbf{z}_i(k) = \begin{bmatrix} r_i(k) + w_{r_i}(k) \\ \theta_i(k) + w_{\theta_i(k)} \end{bmatrix}; \quad i = 1, \ldots .N, \tag{4}$$

where $\mathbf{z}_i(k)$ is the measurement vector of m_z dimension (which contains range (r_i) and azimuth (θ_i) corresponding to the target). $w_{r_i}(k)$ and $w_{\theta_i(k)}$ follows Gaussian PDF with zero mean and standard deviation $\sigma_{r_i}^2$ and $\sigma_{\theta_i}^2$ respectively.

The equivalent representation of (4) is,

$$\mathbf{z}_i(k) = \mathbf{H}\mathbf{x}_i(k) + \mathbf{w}_i(k); \quad i = 1, \ldots .N. \tag{5}$$

where $\mathbf{H}$ is the $m_z \times m_x$ measurement transition matrix and $\mathbf{w}_i(k)$ follows Gaussian PDF with zero mean and covariance $\mathbf{R}_z$ which can be represented as,

$$\mathbf{R}_z = E[\mathbf{w}_i(k)\mathbf{w}_i(k)^T] \tag{6}$$

As shown in Fig. 2, in the presence of ECM the above measurement model is as given in [2],

$$\mathbf{z}_i(k) = \begin{bmatrix} r_i(k) + \Delta r_i(k) + w_{r_i}(k) \\ \theta_i(k) + w_{\theta_i(k)} \end{bmatrix}; \quad i = 1, \ldots .N. \tag{7}$$

The above (7) is equivalent to (1). Where, it is assumed that the target range information deceived by the jammer and as a result i^{th} radar true range is displaced by a value due to RGPO deception $\Delta r_i(k)$. The measurement in the presence of ECM can be modelled as,

$$\mathbf{z}_i(k) = \begin{bmatrix} r_i(k) \\ \theta_i(k) \end{bmatrix} + \mathbf{c}_i(k)\Delta r_i(k) + \begin{bmatrix} w_{r_i}(k) \\ w_{\theta_i(k)} \end{bmatrix}; \quad i = 1, \ldots .N, \tag{8}$$

where, $\mathbf{c}_i(k) \triangleq [1\ 0]^T$. The polar measurements are converted to Cartesian since most trackers work in Cartesian coordinates. It is also assumed that the conversion will not introduce any bias.

For Unbiasedness, the following condition (9) should be satisfied

$$\frac{r_i \sigma_{\theta_i}^2}{\sigma_{r_i}^2} \ll 0.4. \tag{9}$$

Then, ith radar has the measurements

$$\mathbf{z}_i(k) = \mathbf{H}(k)\mathbf{x}_i(k) + \mathbf{B}_i(k)\mathbf{c}_i(k)\Delta r_i(k) + \mathbf{w}_i(k), \tag{10}$$

where, the state vector $\mathbf{x}(k) = [x(k)\ \dot{x}(k)\ y(k)\ \dot{y}(k)]^{\mathrm{T}}$ and

$$\mathbf{H}(k) = \begin{bmatrix} 1 & 0 & 0 & 0 \\ 0 & 0 & 1 & 0 \end{bmatrix} \triangleq \mathbf{H}. \tag{11}$$

The matrix $\mathbf{B}_i(k)$ is a nonlinear function with the true range and azimuth. Using the the measured azimuth $\theta_i^m(k)$ and range $r_i^m(k)$ from radar i, $\mathbf{B}_i(k)$ can be written as given in [13],

$$\mathbf{B}_i(k) = \begin{bmatrix} \cos\theta_i^m(k) & -r_i^m \sin\theta_i^m(k) \\ \sin\theta_i^m(k) & r_i^m \cos\theta_i^m(k) \end{bmatrix}. \tag{12}$$

In the above, superscript m represents measured value. Finally, the new covariance matrix of the measurements in Cartesian coordinates (omitting index k in the measurements for clarity) can be written as,

$$\mathbf{R}_{z_i} = \begin{pmatrix} r_i^2\sigma_{\theta_i}^2 \sin^2\theta_i + \sigma_{r_i}^2 \cos^2\theta_i & (\sigma_{r_i}^2 - r_i^2\sigma_{\theta_i}^2)\sin\theta_i\cos\theta_i \\ (\sigma_{r_i}^2 - r_i^2\sigma_{\theta_i}^2)\sin\theta_i\cos\theta_i & r_i^2\sigma_{\theta_i}^2\cos^2\theta_i + \sigma_{r_i}^2\sin^2\theta_i \end{pmatrix}.$$

However, one can use the observed range and azimuth as well.

C. NOISE JAMMING

The jamming to signal ratio can be obtained as derived in [30]: The received power at the radar can be expressed as,

$$P_{rx} = \frac{P_{tx} G_{tx} G_{rx} \lambda_x^2 \sigma_x}{(4\pi)^3 R_x^4 L_s} \tag{13}$$

where, P_{tx} is the peak transmitted power in watts, G_{tx} is the gain of the transmit antenna, G_{rx} is the gain of the receive antenna, λ_x is the carrier wavelength in meters, σ_x is the radar cross section of the target in square meters, R_x is the range from the radar to the target in meters, and L_s is the total receiver system losses.

The total power received at the radar from the jammer is given by,

$$P_{jr} = \frac{P_{jx} G_{jx} G_{jr} \lambda_x^2}{(4\pi)^2 R_j^2 L_{jr}} \tag{14}$$

where, P_{jx} is the peak transmitted jammer power in watts, G_{jx} is the gain of the jammer antenna, G_{jr} is the gain of the radar antenna in the direction of the jammer, λ_x is the carrier wavelength in meters, R_j is the range from jammer to the radar in meters, and L_{jr} is the total jammer related losses.

Considering the ratio of jammer power (P_{jr}) to radar received power (P_{rx}), the jamming to signal ratio (JSR) can be written as,

$$JSR = 4\pi * \frac{P_{jx} G_{jx} G_{jr} R_x^4 L_s}{P_{tx} G_{tx} G_{rx} \sigma_x R_j^2 L_{jr}} \tag{15}$$

The received noise power at the radar under noise jamming is given by,

$$\sigma_{np}^2 = kT_0 B_n + P_{jr} \tag{16}$$

where, kT_0B_n is the thermal noise of the radar receiver and P_{jr} is the received jammer power which can be computed using (14). Here, k is the Boltzmann's constant ($1.3803 \times 10^{23} J/K$), T_0 is the absolute temperature in Kelvin, and B_n is the noise bandwidth. The increased level in the received jamming power at the radar receiver results in the raise of the noise floor and subsequently leads to the missed detections [28]. When noise power of the jammer is sufficiently higher, it yields false measurements which can be written as,

$$Z_k = \left[z_k^{fa_1}, z_k^{fa_2}, \ldots, z_k^{fa_M} \right] \tag{17}$$

where, M indicates the number of false alarms. Each false alarm's range value is determined by the range bin at which noise power exceeds the threshold provides false detection. Effective signal processing techniques such as space time adaptive processing [31], [32], adaptive beam-forming [33], waveform matching [34] and other advanced filtering techniques [35] are proposed in the literature for the detection and suppression of the noise jamming. In this work, it is assumed that noise jamming is suppressed at signal processing level and measurements are corrupted by RGPO deception jamming only.

Generally, the jamming power will be higher compared to the radar signal power, which helps the jammer to deceive the radar. Few signal processing based techniques like waveform diversity method and singular spectrum analysis for countering the RGPO ECM are presented in [36], [37]. This work aimed at estimating the range deception parameter in a networked radar scenario by using sequential fusion based approach and correct the local tracks by providing feedback information from the fusion center. Instead of detecting the attack, this work aimed to estimate the true target tracks from the falsified track information.

D. OBSERVATIONS

We can clearly see that the range measurement of radar-i is deceived. This deception results in a false track, as shown in Fig. 3a, after performing the distributed tracking. The objectives of the proposed research work are:

1) The measurements are being processed by the local tracker and provide the local estimates (estimated state and covariance). At the fusion center, only local estimates are available, and no other data is available from the radar or tracker. Hence, we need to recreate the measurements at the fusion center by using the local tracks. This recreation of measurements is possible by evaluating the tracklets [38].
2) One needs to formulate a method to associate the local tracks pertaining to the same target so that those tracks can be utilized as a reference to estimate the deception occurrence in other tracks. This association can be formulated as a track-to-track association and can be solved using S-Dimensional (S-D) assignment [39].
3) The deception parameter of the RGPO ECM track is to be estimated by using un-corrupted local tracks. These uncorrupted local tracks can be fused to generate a reference measurement.

III. DISTRIBUTED TRACKING AND TRACK-TO-TRACK ASSOCIATION

A. DISTRIBUTED TRACKING

All radars are deployed with local trackers as shown in Fig. 2. The radar is ignorant about the measurement pertaining to the target, whether it is a true measurement or false measurements due to ECM. The tracker works with the converted measurements. For the acquired measurement, the local tracker provides the local estimates (estimated state and covariance). Given the previous state estimate $\hat{\mathbf{x}}^i(k|k)$, the KF state prediction for $i = 1, \ldots .N$ radars is written as,

$$\hat{\mathbf{x}}^i(k+1|k) = \mathbf{F}\hat{\mathbf{x}}^i(k|k), \tag{18}$$

where k is the discrete time instant and $\mathbf{F}$ is a state transition matrix. Similar to the state prediction, for the given covariance $\mathbf{P}(k|k)$ at the k^{th} instant, the predicted covariance at the $k+1^{th}$ instant is represented as,

$$\mathbf{P}^i(k+1|k) = \mathbf{F}\mathbf{P}^i(k|k)\mathbf{F}^T + \Gamma_x \mathbf{Q}_x \Gamma_x^T, \tag{19}$$

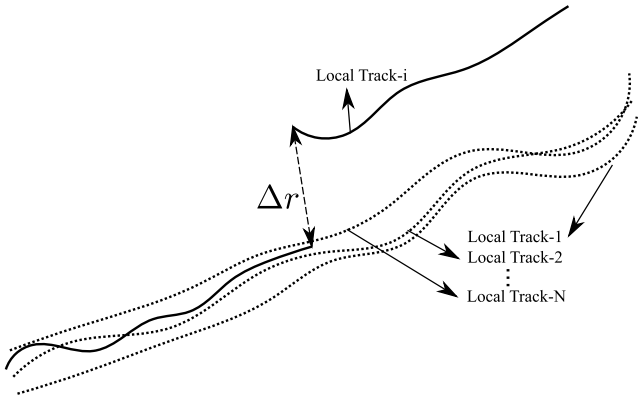

(a) i^{th} local track is deceived by the ECM in single-target multiple-radar case.

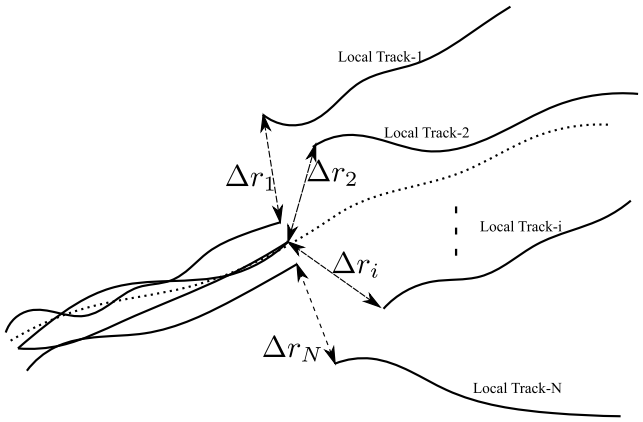

(b) All local tracks deceived by the ECM in single-target multiple-radar case.

FIGURE 3. The local tracks affected by ECM.

where $\mathbf{Q}_x$ is the process noise covariance and Γ is the noise gain matrix as given in [40].

The measurement prediction is,

$$\hat{\mathbf{z}}^i(k+1) = \mathbf{H}(k+1)\hat{\mathbf{x}}^i(k+1|k) \tag{20}$$

The innovation of the filter is,

$$v_z^i(k+1) = \mathbf{z}^i(k+1) - \mathbf{H}(k+1)\hat{\mathbf{x}}^i(k+1|k) \tag{21}$$

The updated state is designated as,

$$\hat{\mathbf{x}}^i(k+1|k+1) = \hat{\mathbf{x}}^i(k+1|k) + \mathbf{W}^i(k+1)v_z^i(k+1), \tag{22}$$

where, $\mathbf{W}^i(k+1)$ is the Kalman gain and is computed as,

$$\mathbf{W}^i(k+1) = \mathbf{P}^i(k+1|k)\mathbf{H}(k+1)^T\mathbf{S}^i(k+1)^{-1}, \tag{23}$$

where, $\mathbf{S}^i$ is the innovation covariance and is represented as,

$$\mathbf{S}^i(k+1) = \mathbf{H}(k+1)\mathbf{P}^i(k+1|k)\mathbf{H}(k+1)^T + \mathbf{R}_z^i. \tag{24}$$

Here $\mathbf{R}_z$ is the measurement covariance matrix. Finally, the updated covariance matrix is given by,

$$\mathbf{P}^i(k+1|k+1) = \mathbf{P}^i(k+1|k) - \mathbf{W}^i(k+1)\mathbf{S}^i(k+1) \times \mathbf{W}^i(k+1)^T. \tag{25}$$

In a single RGPO ECM case, out of all the local tracks, only one track (local track-i) is falsified by the RGPO ECM as illustrated in Fig. 3a. Here, we can see that the local track corresponding to local track-i is deviated by Δr_i from its true position as comprehensively derived in [41]. One has to perform track-to-track association to all local tracks, and it should report that all local tracks correspond to same-origin except i^{th} track. In another case, if N jammers are employed to deceive all the local tracks, the local tracks appear as Fig. 3b. In this case, one should report that all the tracks are from a different origin. The track-to-track association is presented in the subsequent section to address this issue.

B. TRACK-TO-TRACK ASSOCIATION (T2TA)

The fusion of target tracks from multiple sensors is an essential block in the sensor fusion field. The information from multiple sensors has the potential to significantly improve tracking accuracy and target acquisition rates. Out of all the variants of track-to-track associations [42], the hypothesis based track-to-track association is popular and can provide improved tracking accuracy even with less target detection probability and high false alarm rates. The N radars will have their own number of tracks in the form of target estimate $\hat{\mathbf{x}}_{n_i}^i$ with their errors distributed as zero-mean Gaussian with covariance $\mathbf{P}_{n_i}^i$. The $i = 1, 2, \ldots, N$, represents radar number and $n_i = 1, 2, \ldots, T$ represents number of tracks that the each radar generates. To find out the tracks that represents the same target, it is required to perform the likelihood ratio test, given by

$$\chi(H^1_{n_1,n_2,\ldots,n_N} : H^0_{n_1,n_2,\ldots,n_N}) = \frac{\Lambda(H^1_{n_1,n_2,\ldots,n_N})}{\Lambda(H^0_{n_1,n_2,\ldots,n_N})}, \tag{26}$$

where, $\Lambda(H^1_{n_1,n_2,\ldots,n_N})$ represents the likelihood hypothesis of tracks having the common origin, $\Lambda(H^0_{n_1,n_2,\ldots,n_N})$ represents the likelihood hypothesis of tracks coming from the different origin.

Calculating the likelihood hypothesis of tracks having a common origin is as follows:

$$\Lambda(H^1_{n_1,n_2,\ldots,n_N}) = p(\hat{\mathbf{x}}^N_{n_N}, \ldots, \hat{\mathbf{x}}^1_{n_1}|H^1_{n_1,n_2,\ldots,n_N}). \tag{27}$$

The (27) can also be written conditioned on the track estimate of the first radar, given by,

$$\Lambda(H^1_{n_1,n_2,\ldots,n_N}) = p(\hat{\mathbf{x}}^N_{n_N}, \ldots, \hat{\mathbf{x}}^2_{n_2}|H^1, \hat{\mathbf{x}}^1_{n_1})p(\hat{\mathbf{x}}^1_{n_1}|H^1). \tag{28}$$

The $p(\hat{\mathbf{x}}^1_{n_1}|H^1)$ is independent of $H^1_{n_1,n_2,\ldots,n_N}$, hence it can be relaxed. Also, it is assumed to follow uniform distribution, which is a valid assumption in the presence of lack of information. i.e.,

$$p(\hat{\mathbf{x}}^1_{n_1}|H^1_{n_1,n_2,\ldots,n_N}) = p(\hat{\mathbf{x}}^1_{n_1}) = \frac{1}{C}. \tag{29}$$

Substituting, (29) into (28) results in

$$\Lambda(H^1_{n_1,n_2,\ldots,n_N}) = \frac{1}{C}p(\hat{\mathbf{x}}^N_{n_N}, \ldots, \hat{\mathbf{x}}^2_{n_2}|H^1, \hat{\mathbf{x}}^1_{n_1}). \tag{30}$$

Consider the two radar (i, j) case having two tracks (n_i, n_j) as common target origin. Under the Gaussian assumption, if the tracks $\hat{\mathbf{x}}^i_{n_i}$ and $\hat{\mathbf{x}}^j_{n_j}$ at radar i and radar j results from the same target, the likelihood function of the two tracks is given by,

$$\Lambda(H_{n_1,n_2}) = \frac{1}{C}N(\hat{\mathbf{x}}^i_{n_i} - \hat{\mathbf{x}}^j_{n_j}; 0, P^i_{n_i} + P^j_{n_j} - P^{i,j}_{n_i,n_j} - (P^{i,j}_{n_i,n_j})^T), \tag{31}$$

where, $N(\mathbf{x}; \bar{\mathbf{x}}, P)$ represents Gaussian distribution of variable $\mathbf{x}$ has mean and covariance as $\bar{\mathbf{x}}$, P, respectively.
Similar to (31), the generalized likelihood function of all the common tracks (zero error tracks) $n_1, n_2, \ldots, n_N$ for all N radars is given by

$$\Lambda(H^1_{n_1,n_2,\ldots,n_N}) = \frac{1}{C}N(\hat{\mathbf{x}}, 0, P). \tag{32}$$

Here,

$$\hat{\mathbf{x}} = \left[\tilde{\mathbf{x}}^{21}, \quad \tilde{\mathbf{x}}^{31}, \quad \ldots, \quad \tilde{\mathbf{x}}^{N1}\right]^T, \tag{33}$$

where, $\tilde{\mathbf{x}}^{ij}$ represents the difference of the estimates resulted from the same target at i^{th} and j^{th} radar, given by

$$\tilde{\mathbf{x}}^{ij} = \hat{\mathbf{x}}^i_{n_i} - \hat{\mathbf{x}}^j_{n_j}. \tag{34}$$

The diagonal elements of $\mathbf{P}$ is given by,

$$\begin{aligned}\mathbf{P}^{i-1,i-1} &= \mathbb{E}[\tilde{\mathbf{x}}^{i1}\tilde{\mathbf{x}}^{i1'}|H^1_{n_1,n_2,\ldots,n_N}],\\ &= \mathbf{P}^1_{n_1} + \mathbf{P}^i_{n_i} - \mathbf{P}^{1,i}_{n_1,n_i} - (\mathbf{P}^{1,i}_{n_1,n_i})' \quad i = 2, \ldots, N\end{aligned} \tag{35}$$

where $\tilde{\mathbf{x}}^{ij}$ is defined in (34).

The diagonal elements of $\mathbf{P}$ is given by,

$$\begin{aligned}\mathbf{P}^{i-1,j-1} &= \mathbb{E}[\tilde{\mathbf{x}}^{i1}\tilde{\mathbf{x}}^{j1'}|H^1_{n_1,n_2,\ldots,n_N}],\\ &= \mathbf{P}^1_{n_1} - \mathbf{P}^{1,j}_{n_1,n_j} - (\mathbf{P}^{1,i}_{n_1,n_i})' + \mathbf{P}^{i,j}_{n_i,n_j},\\ &\quad i, j = 2, \ldots, N\end{aligned} \tag{36}$$

Similar to (32), the likelihood hypothesis of tracks coming from different origins follows the same procedure as above, given by

$$\begin{aligned}\Lambda(H^0_{n_1,n_2,\ldots,n_N}) &= p(\hat{\mathbf{x}}^N_{n_N}, \ldots, \hat{\mathbf{x}}^2_{n_2}|H^0, \hat{\mathbf{x}}^1_{n_1})p(\hat{\mathbf{x}}^1_{n_1}|H^0)\\ &= \prod_{i=2}^{N} p(\hat{\mathbf{x}}^i_{n_i}|H^0, \hat{\mathbf{x}}^1_{n_1})p(\hat{\mathbf{x}}^1_{n_1}|H^0)\end{aligned} \tag{37}$$

Similar to (29), the $p(\hat{\mathbf{x}}^1_{n_1}|H^0_{n_1,n_2,\ldots,n_N})$ is assumed as diffuse prior given by,

$$p(\hat{\mathbf{x}}^1_{n_1}|H^0_{n_1,n_2,\ldots,n_N}) = p(\hat{\mathbf{x}}^1_{n_1}) = \frac{1}{C}, \tag{38}$$

whereas, $p(\hat{\mathbf{x}}^N_{n_N}, \ldots, \hat{\mathbf{x}}^2_{n_2}|H^0, \hat{\mathbf{x}}^1_{n_1})$ is assumed to follow Poisson distribution in the state space having the spatial density λ. Therefore, substituting (38) into (37) yields

$$\Lambda(H^0_{n_1,n_2,\ldots,n_N}) = \frac{1}{C}\lambda^{N-1}. \tag{39}$$

Finally, from (26), (32), (39), the likelihood ratio test is given by,

$$\chi(H^1_{n_1,n_2,\ldots,n_N} : H^0_{n_1,n_2,\ldots,n_N}) = \frac{\frac{1}{C}N(\hat{\mathbf{x}}, 0, P)}{\frac{1}{C}\lambda^{N-1}} = \frac{N(\hat{\mathbf{x}}, 0, P)}{\lambda^{N-1}}, \tag{40}$$

For T2TA, let us define the track-to-track assignment algorithm of assigning the N_i tracks resulted from N radars representing the same target. For that, define the binary assignment variable

$$\psi_{i_1,i_2,\ldots,i_N} = \begin{cases} 1; & \text{tracks } i_1, i_2, \ldots, i_N \text{ from same target} \\ 0; & \text{from different target} \end{cases}$$

The multidimensional (S-D) track to track assignment algorithm of finding the most likely hypothesis is the result of the constrained optimization problem given below

$$\begin{aligned}\min_{\psi_{i_1,i_2,\ldots,i_N}} & \sum_{i_1=0}^{T_1}\sum_{i_2=0}^{T_2}\cdots\sum_{i_N=0}^{T_N} c_{i_1,i_2,\ldots,i_N}\psi_{i_1,i_2,\ldots,i_N}\\ \text{subject to } & \sum_{i_2=0}^{T_2}\cdots\sum_{i_N=0}^{T_N}\psi_{j,i_2,\ldots,i_N} = 1, \quad j = 1, 2, \ldots, T_1\\ & \sum_{i_1=0}^{T_1}\sum_{i_3=0}^{T_3}\cdots\sum_{i_N=0}^{T_N}\psi_{i_1,j,i_3,\ldots,i_N} = 1,\\ & j = 1, 2, \ldots, T_2\\ & \vdots\\ & \sum_{i_1=0}^{T_1}\cdots\sum_{i_{N-1}=0}^{T_{N-1}}\psi_{i_1,\ldots,i_{N-1}} = 1,\\ & j = 1, 2, \ldots, T_N\end{aligned} \tag{41}$$

and

$$\begin{aligned}\psi_{i_1,\ldots,i_N} &\in \{0, 1\},\\ i_1 &= 0, 1, \ldots, T_1,\\ &\vdots\\ i_N &= 0, 1, \ldots, T_N\end{aligned}$$

The cost function $c_{i_1,i_2,\ldots,i_N}$ in (41) can be calculated as

$$c_{i_1,i_2,\ldots,i_N} = -\ln\chi(H^1 : H^0). \tag{42}$$

where, $\chi(H^1 : H^0)$ is the likelihood ratio given in (40)

C. OBSERVATIONS

After performing the Track to Track Association (T2TA), two cases are possible:

1) In the first case, out of all N local tracks, M local tracks are affected by the ECM as shown in Fig. 3a, where $N - M \geq 2$. That means at least two local tracks are uninfluenced by the ECM. In this case, the unaffected local tracks are fused to form a reference track. This reference track can be further used to estimate the deception parameter of other radars. However,

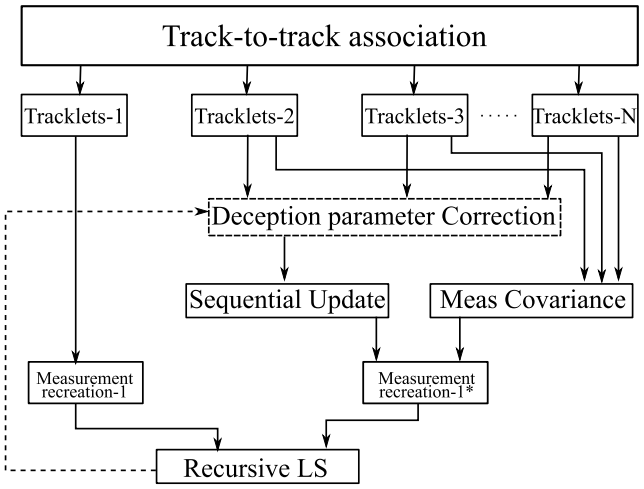

FIGURE 4. The block diagram representation of overall flow of the proposed algorithm.

this solution is sub-optimal since there is a constrain on the number of local tracks that are deceiving, and fusion is limited to $N-M$ local tracks. By considering only $N-M$ local tracks, we are losing the valuable information being available in M local tracks.

2) In the second case, all the local tracks are affected by RGPO ECM, as shown in Fig. 3b. All the reported local tracks are different, and none of them are associated. In this case, the tracks are first compensated by the previously estimated deception parameter and fused to form a reference track. Thereafter, the deception parameter of other local tracks is calculated. This algorithm provides a generalized solution irrespective of the number of RGPO jammers.

IV. DECEPTION PARAMETER ESTIMATION ALGORITHM

The block diagram for the overall flow of the proposed algorithm is as shown in Fig. 4. As observed in the previous section, in case of all the local tracks are deceived, there is no availability of local tracks to fuse and form a reference track. In the first step of the algorithm, measurement recreation is carried out for deceived track in the tracklets framework. On the other hand, the tracklets are computed for the rest of the tracks. These tracklets are compensated using previously estimated deception parameters (In the Fig. 4 the feedback of previous estimates is shown in dotted lines). Next, the sequential update algorithm is applied to the compensated local tracks to obtain the fused states and covariance. Using the fused states, the fused measurement (reference measurement) is recreated. Further, perform RLSE by utilizing the recreated measurement of deceived track and the reference measurement.

A. MEASUREMENT RECREATION OF DECEIVING TRACK

The local tracker provides the updated states and covariances. However, the measurements are being corrupted by the deception parameter. Hence, one needs to recreate the measurements. Once the measurement covariance is known or estimated (i.e. $\hat{\mathbf{R}}_z$), we can rewrite the Kalman gain (23) as,

$$\begin{aligned}\hat{\mathbf{W}}(k+1) &= \mathbf{P}(k+1|k)\mathbf{H}(k+1) \\ &\quad \cdot [\hat{\mathbf{R}}_z(k+1) + \mathbf{H}(k+1)\mathbf{P}(k+1|k)\mathbf{H}(k+1)^T]^{-1}.\end{aligned} \tag{43}$$

The (23) can be rewritten as,

$$\mathbf{x}(k+1|k+1) - \mathbf{F}\mathbf{x}(k|k) = \hat{\mathbf{W}}[\mathbf{y}(k+1) - \mathbf{H}\mathbf{F}\hat{\mathbf{x}}(k|k)], \tag{44}$$

where, $\mathbf{y}(k+1)$ is the recreated measurement. Here on the right hand side, gain matrix should be taken to the left side and perform the pseudo inversion as,

$$\hat{\mathbf{W}}(k+1)^{-1} = (\hat{\mathbf{W}}(k+1)^T\hat{\mathbf{W}}(k+1))^{-1}\hat{\mathbf{W}}(k+1)^T, \tag{45}$$

Upon rearranging, the recreated measurement can be found as,

$$\begin{aligned}\mathbf{y}(k+1) = \mathbf{W}(k+1)^{-1}[\hat{\mathbf{x}}(k+1) - (I - \mathbf{W}(k)\mathbf{H}(k)) \\ \times \mathbf{F}(k)^T\hat{\mathbf{x}}(k)]\end{aligned} \tag{46}$$

At this stage, to successfully recreate the measurements, we need $\hat{\mathbf{R}}_z$. To estimate the $\hat{\mathbf{R}}_z$, we are using Tracklets framework [43]. This method constructs the approximately uncorrelated equivalent measurements and the associated covariance matrices from the local tracks. The inverse Kalman filter-based tracklet method from [44] is used. Based on this method, the equivalent measurement vector $\mathbf{u}(k+1,k)$ and measurement covariance $\mathbf{U}(k+1,k)$ can be found using Algorithm-1,

Algorithm 1 Measurement Recreation Using Tracklets

1: inputs:$\mathbf{x}(k|k)$, $\mathbf{P}(k|k)$, $\mathbf{x}(k+1|k+1)$, $\mathbf{P}(k+1|k+1)$
2: At time k
3: **Compute Predictions**

$$\begin{aligned}\mathbf{x}(k+1|k) &= \mathbf{F}\mathbf{x}(k|k) \\ \mathbf{P}(k+1|k) &= \mathbf{F}\mathbf{P}(k|k)\mathbf{F}^T + \mathbf{Q}_x\end{aligned}$$

4: **Compute**

$$\begin{aligned}\mathbf{A}(k+1,k) = \mathbf{P}(k+1|k)[\mathbf{P}(k+1|k) \\ - \mathbf{P}(k+1|k+1)]^{-1}\end{aligned}$$

5: **Compute pseudo-measurement**

$$\begin{aligned}\mathbf{u}(k+1,k) = \hat{\mathbf{x}}(k+1|k) + \mathbf{A}(k+1|k)[\hat{\mathbf{x}}(k+1|k+1) \\ - \hat{\mathbf{x}}(k+1|k)],\end{aligned}$$

6: **Compute pseudo-measurement covariance**

$$\mathbf{U}(k+1,k) = [\mathbf{A}(k+1,k) - I]\mathbf{P}(k+1|k).$$

The detailed derivation of the tracklets is presented in the [45] and [46]. We constructed equivalent measurement vector $\mathbf{u}(k+1,k)$ and its error covariance matrix $\mathbf{U}(k+1,k)$. Note that, in order to calculate $\mathbf{u}(k+1,k)$ using $\hat{\mathbf{x}}_f(k+1|k)$ and $\mathbf{P}_f(k+1|k)$, one needs the estimated target state $\hat{\mathbf{x}}(k|k)$ and its covariance matrix $\mathbf{P}(k|k)$.

B. CORRECTION OF DECEPTION PARAMETER AMONG ALL TRACKS

Consider a case, where N RGPO ECM jammers are employed to perform RGPO ECM to all the N local tracks and results in N deceived local tracks. Here, all tracks gets altered due to RGPO ECM and the deception parameter for each track has to be estimated. In this case, the track-to-track association reports all the tracks are unique and they are not from the same origin. Therefore, each track is to be first compensated with the estimated range deception parameter (Δr_i) obtained in the previous scans and fuse the compensated tracks to get a fused state and covariance.

The equivalent measurement is $\hat{\mathbf{u}} = [\hat{x}, \hat{y}]$. Since the equivalent measurement is in Cartesian, one can get the measurement in polar by applying transformation. Therefore, compensate the range in the converted equivalent measurement as

$$r_c(k+1) = \sqrt{\left(\hat{x}(k+1)\right)^2 + \left(\hat{y}(k+1)\right)^2} - \Delta r(k) \tag{47}$$

Here, $\Delta r(k)$ is the previous estimate and c indicates the corrected measurement.

$$\theta_c(k+1) = \arctan\left(\frac{\hat{y}(k+1)}{\hat{x}(k+1)}\right) \tag{48}$$

These corrected polar measurements can be again transformed to Cartesian by standard coordinate conversion without bias as

$$x_m(k+1) = b^{-1} r_c(k+1)\cos(\theta_c(k+1))$$
$$y_m(k+1) = b^{-1} r_c(k+1)\sin(\theta_c(k+1))$$

where, $b \triangleq e^{-\sigma^2_{\theta_c}/2}$. Now these x_m and y_m serve as the local tracker information without being effected by the ECM. Hence in this case, to find the deception of track-i, all the tracks are compensated except i^{th} track. Therefore, the sequential fusion runs for $N-1$ tracks.

C. CONSTRUCTING THE REFERENCE MEASUREMENT

Now the goal is to create reference measurement by fusing $N-1$ tracks, which are compensated by the previously estimated deception parameters. The sequential update algorithm is performed in the fusion step. Although it is not an optimal approach for fusing the local tracks, it is computationally inexpensive than parallel update method [47]. In addition, it is independent of previous equivalent measurements at time instant k. Therefore, the index for sequential fusion is $j = 1, \ldots .N-1/i$. Which means j runs for all tracks rather than effected track i. After calculating the equivalent measurements for all the $(N-1)$ local tracks, we get $\left\{\mathbf{u}(k+1)^j, \mathbf{U}(k+1)^j\right\}_{j=1}^{N-1}$. This tracklet computation using Algorithm-1. It is assumed that fused state and covariance at k^{th} instant is available as $\hat{\mathbf{x}}_f(k|k)$ and $\hat{\mathbf{P}}_f(k|k)$ respectively. The sequential updation algorithm is presented in Algorithm-2. In the algorithm, all $N-1$ local tracks are sequentially updated to provide $\mathbf{x}_f(k+1|k+1)$ and $\mathbf{P}_f(k+1|k+1)$. One of the advantages of this sequential fusion approach is that in each "for loop" (step-5 in Algorithm-2) only a low dimensional Kalman filter that is independent of the size of the stacked RGPO vector and number of the sensors is needed. Furthermore, the fusion of local tracks can be accomplished by adding one sequential update for the latest corrected measurement of sensor j to the previously fused track. In the sequential fusion algorithm, it is also important to note that, there is no constraint on the rate at which local tracks are being received from the individual sensors.

Algorithm 2 Sequential Update Algorithm

1: inputs: $\left\{\hat{\mathbf{x}}^j(k|k), \mathbf{P}^j(k|k)\right\}_{j=1}^{N-1}$
2: At time k
3: **Compute** $\hat{\mathbf{x}}_f(k+1|k)$ and $\hat{\mathbf{P}}_f(k+1|k)$ using

$$\hat{\mathbf{x}}_f(k+1|k) = \mathbf{F}\hat{\mathbf{x}}_f(k|k)$$
$$\hat{\mathbf{P}}_f(k+1|k) = \mathbf{F}\hat{\mathbf{P}}_f(k|k)\mathbf{F}^T + \mathbf{Q}_x$$

4: **Initialize**

$$\hat{\mathbf{x}}^0(k+1|k+1) \triangleq \hat{\mathbf{x}}_f^j(k+1|k)$$
$$\mathbf{P}^0(k+1|k+1) \triangleq \mathbf{P}_f^j(k+1|k)$$

5: **for** `j=1:N-1` **do**
6: The state update is given by,

$$\hat{\mathbf{x}}^j(k+1|k+1) = \hat{\mathbf{x}}^{j-1}(k+1|k+1) + \mathbf{W}^j(k)\mathbf{x}^j(k+1) - \mathbf{H}^j(k+1)\hat{\mathbf{x}}^{j-1}(k+1|k+1)$$

7: The gain is given by,

$$\mathbf{W}^j(k+1) = \mathbf{P}^{j-1}(k+1|k+1)\mathbf{H}^j(k+1)^T[\mathbf{H}^j(k+1) \times \mathbf{P}^{j-1}(k+1|k+1)\mathbf{H}^j(k+1)^T + \mathbf{R}_z^j(k+1)]^{-1}$$

8: The covariance is given by,

$$\mathbf{P}^j(k+1|k+1) = \mathbf{P}^{j-1}(k+1|k+1) - \mathbf{W}^j(k+1) \times \mathbf{S}^j(k+1)\mathbf{W}^j(k+1)^T$$

9: **end for**
10: The final updated state estimate and covariance values are

$$\hat{\mathbf{x}}_f(k+1|k+1) = \hat{\mathbf{x}}^{N-1}(k+1|k+1)$$
$$\mathbf{P}_f(k+1|k+1) = \mathbf{P}^{N-1}(k+1|k+1)$$

D. DECEPTION PARAMETER ESTIMATION ALGORITHM

The algorithm for estimating the deception parameter is presented in Algorithm-3. Also, the block diagram representation of deception parameter estimation is shown in Fig. 4.

Algorithm 3 Deception Parameter Estimation Algorithm

1: **for** $i = 1 : N$ **do**

2: **Recreate measurements:** The tracklets for the deceived track are computed and then recreate the measurements corresponding to local tracks-i using (45),we obtain $\mathbf{y}^i$ as

$$\begin{aligned}\mathbf{y}^i(k+1) = \mathbf{W}^i(k+1)^{-1}[\hat{\mathbf{x}}^i(k+1|k+1) \\ -(I-\mathbf{W}^i(k+1)\mathbf{H}(k+1))\mathbf{F}^T\hat{\mathbf{x}}^i(k|k)]\end{aligned}$$

3: **Fused state and covariance:** Compute the tracklets for $N-1$ tracks using Algorithm-1 and compensate them using Subsection-IV-B. For the compensated tracks, perform sequential update using Algorithm-2, to get fused state $\hat{\mathbf{x}}_f(k+1|k+1)$ and fused covariance $\hat{\mathbf{P}}_f(k+1|k+1)$.

4: **Fused measurement covariance:**

$$\begin{aligned}\mathbf{R}_f(k+1) = \mathbf{H}(k+1)\left[\sum_{j=1}^{N-1}(\mathbf{U}^j(k+1,k))^{-1}\right]^{-1} \\ \times\mathbf{H}(k+1)^{\mathrm{T}}\end{aligned}$$

5: Calculate the fused weight as

$$\begin{aligned}\mathbf{W}_f(k+1) = \mathbf{P}_f(k+1|k)\mathbf{H}(k+1)^{\mathrm{T}}[\mathbf{H}(k+1) \\ \times\mathbf{P}_f(k+1|k)\mathbf{H}(k+1)^{\mathrm{T}}+\mathbf{R}_f(k+1)]^{-1}.\end{aligned}$$

6: **Reference measurement** Therefore, by providing the fused covariance in (49), we get $\mathbf{y}^{i*}$ as

$$\begin{aligned}\mathbf{y}^{i*}(k+1) = \mathbf{W}_{fk}(k+1)^{-1}[\hat{\mathbf{x}}_f(k+1|k+1) \\ -(I-\mathbf{W}_f(k+1)\mathbf{H}(k+1))\mathbf{F}^T\hat{\mathbf{x}}_f(k|k)]\end{aligned}$$

7: **Compute RLSE:** The new measurement using reference measurement and re-created track is

$$\begin{aligned}\mathbf{y}(k) &= \mathbf{y}^i(k)-\mathbf{y}^{i*}(k) \\ &= \mathbf{H}^i(k)\mathbf{x}^i(k)+\mathbf{B}^i(k)\mathbf{c}^i(k)\Delta r_i(k) \\ &\quad +\mathbf{w}^i(k)-\mathbf{H}^{i*}(k)\mathbf{x}^{i*}(k)-\mathbf{w}^{i*}(k) \\ &= \mathbf{H}(k)\Delta r(k)+\mathbf{w}^i(k)-\mathbf{w}^{i*}(k) \\ &= \mathbf{H}(k)\Delta r+\tilde{w}(k)\end{aligned}$$

recursively solve using the last updates in recursive least squares estimation (RLSE) framework [47].

8: **end for**

V. PERFORMANCE EVALUATION

A. INNOVATION TEST

Innovation test is used for testing the efficiency of RLS estimator. The measurement is given by,

$$\mathbf{y}(k) = \mathcal{H}(k)\Delta\mathbf{r}(k)+\tilde{\mathbf{w}}(k) \tag{49}$$

where, $\mathcal{H}(k)$ measurement transition matrix and the measurement noise covariance is $\mathbf{R}(k) = \mathbf{R}^i(k)+\mathbf{R}^{i*}(k)$.

The innovation covariance is represented as,

$$\mathbf{S}(k) = \mathcal{H}(K)\Sigma(k)\mathcal{H}(k)^T+\mathbf{R}(k) \tag{50}$$

The gain and the residual is calculated as

$$\mathbf{G}(k) = \Sigma(k)\mathcal{H}(k)^T[\mathcal{H}(k)\Sigma(k)\mathcal{H}(k)^T+\mathbf{R}(k)]^{-1} \tag{51}$$

$$\Gamma(k) = y(k)-\mathcal{H}(k)\Delta\hat{r}(k) \tag{52}$$

The range gate estimate and its covariance are,

$$\Delta\hat{r}^i(k) = \Delta\hat{r}^i(k-1)+\mathbf{G}(k)\Gamma(k) \tag{53}$$

$$\begin{aligned}\Sigma(k) = \Sigma(k-1)-\Sigma(k)\mathbf{H}(k)^T \\ \cdot[\mathbf{H}(k)\Sigma(k)\mathbf{H}(k)^T+\mathbf{R}(k)]^{-1} \\ \cdot\mathbf{H}(k)\Sigma(k)\end{aligned} \tag{54}$$

The innovation test [48] is given as,

$$\Gamma(k)\mathbf{S}(k)^{-1}\Gamma(k) \leq \xi^2_{n_r}(1-q) \tag{55}$$

where, $\xi^2_{n_r}(1-q)$ is the chi square value with n_r degree of freedom and tail probability of q.

B. CRAMER RAO LOWER BOUND

The Cramer Rao Lower Bound (CRLB) on the mean square error of unbiased estimator is a frequently used metric for determining the correctness of parameter estimate based on a set of data [49]. The CRLB of the algorithm provides the criterion to know the minimum value of error, that can be achieved by the algorithm.

From the measurement equation of the RLS estimator,

$$\mathbf{y}^i(k) = \mathcal{H}(k)\Delta\mathbf{r}^i(k)+\tilde{\mathbf{w}}_i(k) \tag{56}$$

where $\Delta r_i(k)$ is the range gate vector to be estimated and the measurement noise covariance of $\mathbf{w}_i(k)$ is given as $\mathbf{R}_i(k) = \mathbf{R}_i(k)+\mathbf{R}^*_i(k)$ where $\mathbf{R}_i(k)$ is the measurement noise of i^{th} local track and $\mathbf{R}^*_i(k)$ is the measurement noise obtained by fusing rest of the local tracks.

The covariance matrix of an unbiased estimator is bounded as below [29] and [50]:

$$\mathbb{E}\left\{\left(\Delta\hat{\mathbf{r}}_i(k)-\Delta\mathbf{r}_i\right)\left(\Delta\hat{\mathbf{r}}_i(k)-\Delta\mathbf{r}_i\right)'\right\} \geq \mathbf{J}_\mathbf{z}(k)^{-1} \tag{57}$$

Here, $\mathbb{E}$ is the estimation operator and $\mathbf{J}_z$ is the Fisher Information Matrix(FIM) and is given as

$$\begin{aligned}\mathbf{J}_\mathbf{z}(k) = \mathbb{E}\big\{[\nabla\ln p(\mathbf{y}(k)\mid\Delta\mathbf{r}(k))] \\ \times[\nabla\ln p(\bar{y}(k)\mid\Delta\mathbf{r}(k))]'\big\}_{\Delta\mathbf{r}(k)=\Delta\mathbf{r}_t}\end{aligned} \tag{58}$$

where, Δr_t is the true value of the range gate parameter and ∇ is the gradient operator. Also, $p(\mathbf{y}(k)\mid\Delta r(k))$ is the likelihood function, which is given as below:

$$\begin{aligned}p(\mathbf{y}(k)\mid\Delta r(k)) \\ = \frac{1}{\sqrt{2\pi|\mathbf{R}(k)|}}\cdot\exp\left\{\frac{-1}{2}[\mathbf{y}(k)-\mathcal{H}(k)\Delta r(k)]'\right. \\ \left.\times\ \mathbf{R}(k)^{-1}[\mathbf{y}(k)-\mathcal{H}(k)\Delta r(k)]\right\}\end{aligned} \tag{59}$$

Substituting $\lambda_y = -\ln p(\mathbf{z}(k) \mid \Delta\mathbf{r}(k))$,

$$\lambda_y = \mathrm{C} + \frac{-1}{2}[\mathbf{y}(k) - \mathcal{H}(k)\Delta r(k)]' \mathbf{R}(k)^{-1} \times [\mathbf{y}(k) - \mathcal{H}(k)\Delta r(k)] \tag{60}$$

Upon further simplification,

$$\nabla_{\Delta\mathbf{r}}\lambda_y = \mathcal{H}(k)'\mathbf{R}(k)^{-1}(\mathbf{y}(k) - \mathcal{H}\Delta r(k)) \tag{61}$$

which gives,

$$\mathbf{J}_z(k) = \mathcal{H}(k)'\mathbf{R}(k)^{-1}\mathcal{H}(k) \tag{62}$$

The FIM at K is also the recursive form of CRLB is represented as,

$$\mathbf{J}_z(K) = \sum_{k=1}^{K} \mathbf{J}_z(k) \tag{63}$$

C. NEES TEST AND CONFIDENCE INTERVAL TEST

In simulation frameworks, the normalised estimation error squared (NEES) test can be used to determine if the estimator is efficient, that is, whether the error matches the covariance provided by the CRLB [51]. The error matrix provided by the CRLB is J_z. For an estimated deception parameter $\Delta\hat{r}(k)$, there exist a ground truth $r(k)$. The estimation error is given by,

$$\Delta\tilde{r}(k) = \Delta r(k) - \Delta\hat{r}(k) \tag{64}$$

The NEES value for the parameter Δr is written as,

$$\Delta\tilde{r}^T(k)\mathbf{J}_z(k)\Delta\tilde{r}(k) \leq \xi^2_{n_r}(1-q) \tag{65}$$

The confidence interval of a deception parameter is evaluated for $\Delta r(k)$. The squared norm of the error should be constrained by the estimate if the estimator is efficient [52].

The confidence for the parameter $\Delta r(k)$ is,

$$\Delta\tilde{r}^T(k)\Sigma^{-1}(k)\Delta\tilde{r}(k) \leq \xi^2_{n_r}(1-q) \tag{66}$$

which follows chi square distribution with degree of freedom equal to n_r.

VI. RESULTS

A. SINGLE RADAR SENSOR JAMMING

In this case, a single radar effected by jamming (RGPO ECM) is considered among the three radars present in the surveillance region. All the radars are static and synchronous in time with $t_s = 1$s. The radars are located at r^s and θ^s with reference to the origin. The range and azimuth measurements are corrupted with the noise with a standard deviation of σ_r and σ_θ, respectively. A single target is considered in the surveillance region, and all the radars are comprises of the local tracker to provide local estimates about the target. A single jammer is considered in this simulation, and it influences the single radar equipped with local tracker-1. Since the local track-1 generated from the tracker-1 is deceived with the RGPO ECM measurements, this yields a range displacement of Δr_1. The positions, measurement standard deviation, and

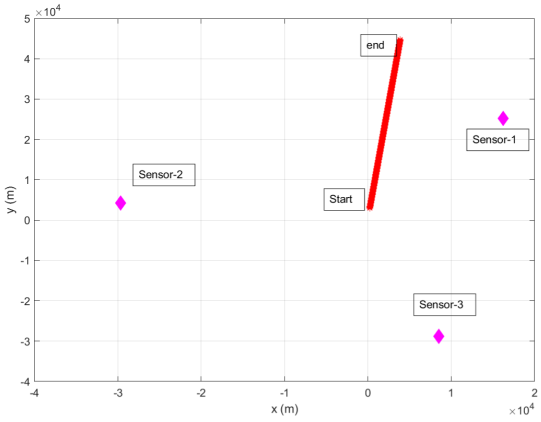

FIGURE 5. Scenario of the static radars and target.

TABLE 1. Radar parameters for single radar jamming case.

	Sensor-1	Sensor-2	Sensor-3
Range (r^s in m)	30000	30000	30000
Azimuth (θ^s in rad)	1	3	5
Std of range (σ_r in m)	20	20	20
Std of azimuth (σ_θ in rad)	1m	1m	1m
Sampling time (t_s in s)	1	1	1
Deception (Δr in m)	1000	-	-

deception parameters are tabulated in the Table-I. Moreover, the scenario is depicted in Fig. 5. The target is located at a range of 3000m and the azimuth of 1.5 rad from the origin. The target moves with a speed of 40m/s, and 80 deg heading throughout the simulation time of 1000s. The target follows a constant velocity model, and the state transition matrix is represented as,

$$F = \begin{bmatrix} 1 & t_s & 0 & 0 \\ 0 & 1 & 0 & 0 \\ 0 & 0 & 1 & t_s \\ 0 & 0 & 0 & 1 \end{bmatrix}.$$

1) TRACKING ACCURACY

A GNN association based EKF filter is used for target tracking. Two-point initialization method [53] is used to initialize the filter. The range-azimuth measurements $r(0)$ and $\theta(0)$ at zero instant are considered to form a converted measurements as $x(0)$ and $y(0)$. Similarly, the first instant measurements are used to form the converted measurements as $x(1)$ and $y(1)$. Hence, the two-point initialization is given by,

$$\mathbf{x} = \begin{bmatrix} x(1) & \dfrac{x(1)-x(0)}{t_s} & y(1) & \dfrac{y(1)-y(0)}{t_s} \end{bmatrix}$$

The measurement conversion follows the unbiased conversion by using,

$$x(1) = \lambda^{-1} r(1)\cos(\theta(1))$$
$$y(1) = \lambda^{-1} r(1)\sin(\theta(1))$$

Here $\lambda = \exp\left(-\frac{\sigma_\theta^2}{2}\right)$. This unbiased conversion is valid for initialization, since it follows the necessary criteria of

$\frac{r\sigma_\theta^2}{\sigma_r} \ll 0.4$. The covariance is initialized using,

$$P(1 \mid 1) = \begin{bmatrix} R_{xx}(1) & \frac{R_{xx}(1)}{t_s} & 0 & 0 \\ \frac{R_{xx}(1)}{t_s} & \frac{2R_{xx}(1)}{t_s^2} & 0 & 0 \\ 0 & 0 & R_{yy}(1) & \frac{R_{yy}(1)}{t_s} \\ 0 & 0 & \frac{R_{yy}(1)}{t_s} & \frac{2R_{yy}(1)}{t_s^2} \end{bmatrix}$$

where,

$$\begin{aligned} R_{xx} &= (\lambda^{-2} - 2)\,(r(1))^2 \cos^2(\theta(1)) \\ &\quad + \frac{((r(1))^2 + \sigma_r^2)}{2}\left(1 + \lambda^4 \cos 2\theta(1)\right) \\ R_{yy} &= (\lambda^{-2} - 2)\,(r(1))^2 \sin^2(\theta(1)) \\ &\quad + \frac{((r(1))^2 + \sigma_r^2)}{2}\left(1 - \lambda^4 \cos 2\theta(1)\right) \end{aligned}$$

The tracking is performed with the help of an extended Kalman filter (EKF). The tunable parameters like process noise covariance and measurement noise covariances as Q_x and R_z, respectively are represented as,

$$Q_x = 0.08 \begin{bmatrix} \frac{1}{3} * (t_s^3) & \frac{1}{2} * (t_s^2) & 0 & 0 \\ \frac{1}{2} * (t_s^2) & t_s & 0 & 0 \\ 0 & 0 & \frac{1}{3} * (t_s^3) & \frac{1}{2} * (t_s^2) \\ 0 & 0 & \frac{1}{2} * (t_s^2) & t_s \end{bmatrix}$$

and

$$R_z = \begin{bmatrix} R_{xx} & R_{xy} \\ R_{yx} & R_{yy} \end{bmatrix}$$

where,

$$R_{xy} = R_{yx} = \left[\frac{\lambda^{-2}(r)^2}{2} + \frac{((r)^2 + \sigma_r^2)\lambda^4}{2} - ((r)^2\right] \sin 2\theta.$$

The tracking performance is evaluated using the PRMSE. The tracking performance of all the local trackers is depicted in Figs. 6a-6c.

It is observed from Fig. 6a that the local track-1 PRMSE is around 1000 ± 8m because of the range deception of 1000m affected by the RGPO ECM jamming. Moreover, the PRMSE of the local track-2 and local track-3 are also depicted in the Fig. 6b and Fig. 6c. The PRMSE of local track-2 and local track-3 is lesser than the local track-1; this is because the RGPO jamming is un-influencing local track-2 and local track-3. This tracking performance can be directly reflected in the fusion module.

2) SEQUENTIAL FUSION PERFORMANCE

The sequential fusion is performed on the compensated equivalent measurements. The correction is performed at k in the polar coordinates with the help of the estimated deception parameter at $k-1$ time instant. For the time stamp of $k = 1$, since there are no previously fused estimates are available, the local track's updated state is considered as the fused state estimate i.e., $\mathbf{x}_f(k|k) = \mathbf{x}(k|k)$ and $\mathbf{P}_f(k|k) = \mathbf{P}(k|k)$ at $k = 1$. It can be seen from the Figs. 6d-6f that, the PRMSE of local track-1 fused estimate is equal to the PRMSE of local track-1 for the initial scan. After that, the deception parameter estimation converges over time and improves the PRMSE of the sequential fusion block. Therefore, we observed that, the local track-1 fusion PRMSE decreases over time, and the similar procedure holds true for local track-2 and local track-3 performance. Since the deception parameter is kept at 1000m for local track-1, the sequential fusion PRMSE starts at 1000m and finally diminishes to 10 m accuracy. The sequential fusion provides sub-optimal solution, but it is a significant technique importance due to its reduced computational requirement. It is also worth noting that the sequential fusion is only dependent on the compensated equivalent measurements to compute the fused state and covariance estimates at a given scan.

3) DECEPTION PARAMETER EVALUATION

The deception parameter is calculated in the RLSE framework. In this framework, measurement i corresponds to the deceived local track i. whereas, the reference measurement is generated by the compensation and fusion of all local tracks except i. That is the sequential fusion block runs for $i^* \in 1, \cdots N/i$. The initial state and covariance of the RLSE is $\Delta r(0|0) = 0$ and $\Sigma(0|0) = 1000^2$. There is no prior information regarding the deception parameter and its associated covariance at $k = 0$. The deception parameter of the deceived local track-1 is estimated, and its corresponding PRMSE is plotted in Fig. 7. Initially, the deception is considered as zero, and hence PRMSE at initial state is equal to 1000 m which is the deception created by the RGPO ECM. Along with the estimated deception parameter, we also plotted the Batch CRLB ($\sqrt{B - CRLB}$), Recursive CRLB ($\sqrt{R - CRLB}$) and the diagonal of the covariance estimate ($\sqrt{\Sigma}$). From Fig. 7, it can be observed that the estimator is working effectively, and the estimated deception parameter is coming closer the CRLB value. We have plotted on logy scale for better visualization, keeping the deception parameter changing from 10^3 to unity.

4) ESTIMATOR PERFORMANCE EVALUATION

The performance of the proposed algorithm is validated using the NEES test, innovation test, and confidence interval test. In all three tests, we have considered chi-square distribution as $\chi_b^2(1-q)$ where q is tail probability. We have taken q as 1% and 5% and is plotted in the Fig. 8. It is evident from the results that the NEES values are falling within the chi-square distribution with a tail probability of 5% which infers that the proposed estimator is efficient. The NEES for the estimator along with the chi-square distribution is shown in Fig. 8a. Further, it can be observed from Fig. 8b that the innovation test is inbound with the Raleigh distribution, and it is falling within the 95% confidence interval of the chi-square

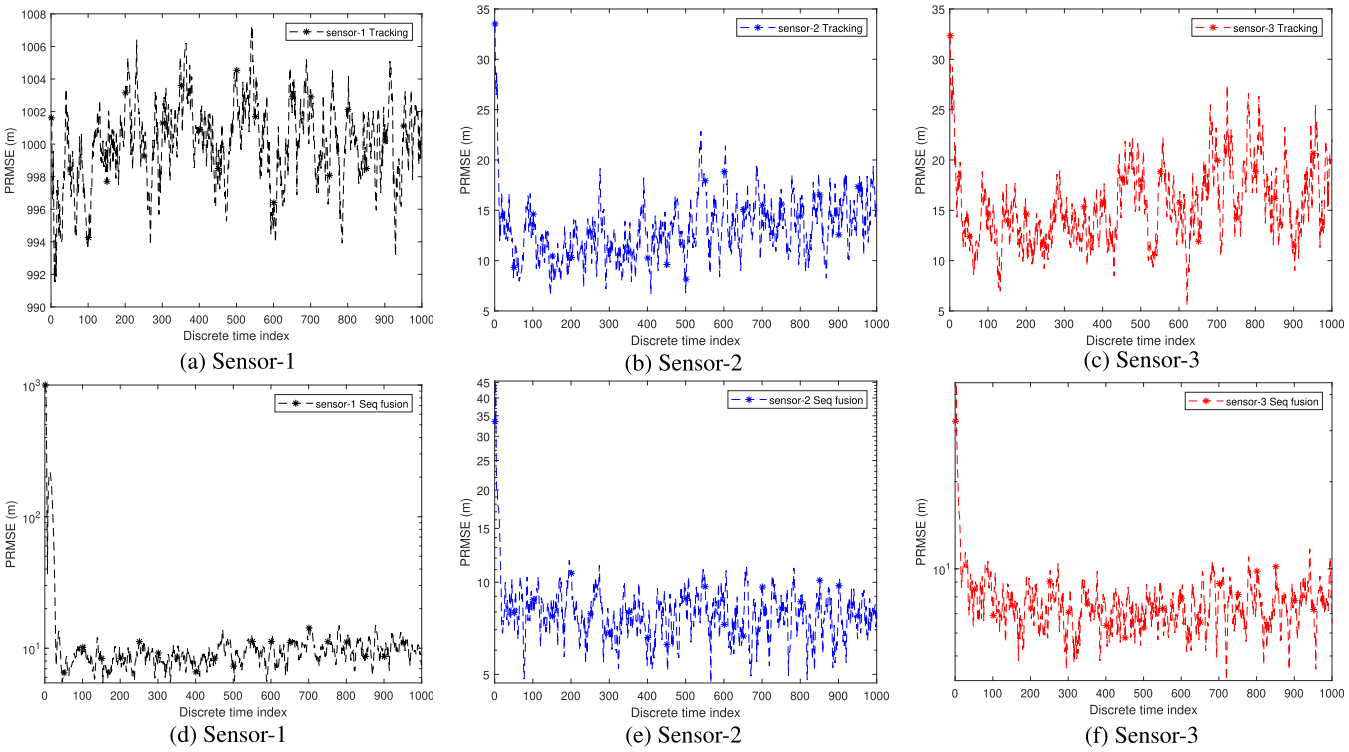

FIGURE 6. (a-c) Tracking performance, (d-f) Sequential fusion performance.

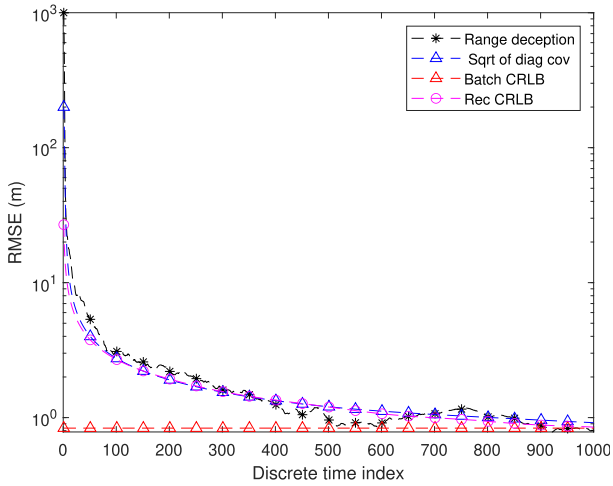

FIGURE 7. Deception parameter of local track-1.

distribution with a degrees of freedom equal to two. Further, we examined the confidence area of the parameter to associated confidence interval, which intuitively specifies whether the estimated parameter and the estimated parameter covariance are agreeing with each other. From Fig. 8c it is evident that the confidence region of the estimated parameter is well within the specified range. That is the estimated covariance and R-CRLB are almost equal. Therefore, we can state that the proposed estimator neither optimistic nor pessimistic.

B. MULTI-SENSOR JAMMING

In this scenario, we considered three radars present in the surveillance region and all are affected by RGPO ECM. All

TABLE 2. Sensor parameters for multiple sensor jamming case.

	Sensor-1	Sensor-2	Sensor-3
Range (r_i^s in m)	30000	30000	30000
Azimuth (θ_i^s in rad)	1	3	5
Std of range (σ_{r_i} in m)	50	100	150
Std of azimuth (σ_{θ_i} in rad)	1m	2m	3m
Sampling time (t_s in s)	1	1	1
Deception (Δr_i in m)	1000	1500	2000

the three radars are assumed to be static and synchronous in time. The radars are located at r_i^s and θ^s with respect to origin. The range and azimuth measurements are corrupted with white Gaussian noise with zero mean and standard deviations of σ_{r_i} and σ_{θ_i} respectively. A single target is considered, and all local trackers provide updated state and covariance to the fusion center. Unlike the single jammer three jammers are considered, and this yields a range displacement of Δr_i to each local track. The locations, standard deviation of measurements, and deception parameters of each of the local track are tabulated in Table-II.

1) TRACKING ACCURACY

A two-point initialization method is adapted to initialize the filter, the extended Kalman filter is used to filter the measurements. The tracking PRMSE of all the three local tracks is depicted in Figs. 9a-9c. Since all the three local tracks are affected by the jamming, we can observe that the local track-1 PRMSE is around 1000m; this is as a result of range deception parameter of 1000m effected to the local track. Similarly, the PRMSE of local track-2 and local track-3 are 1500m and 2000m, respectively. Corresponding to its RGPO, since all the tracks are deceived; this results in hypothesis $H1$ in T2TA.

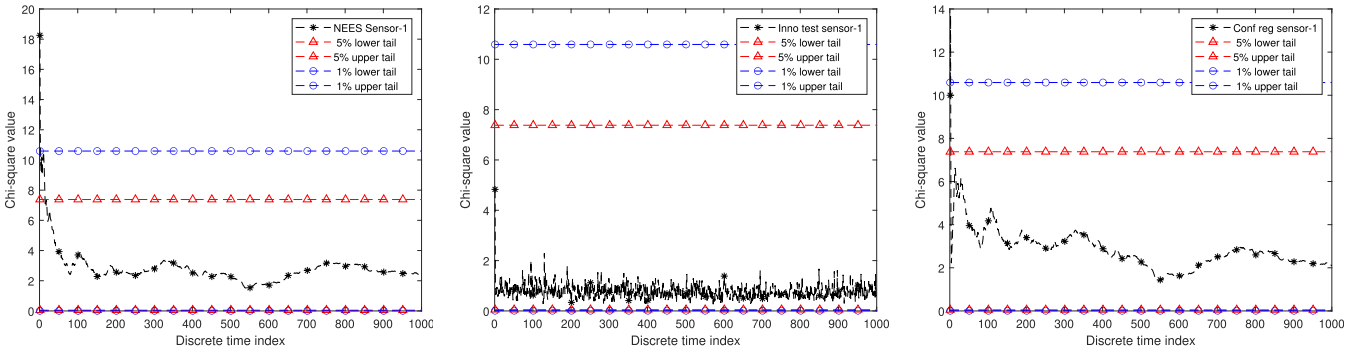

(a) Sensor-1 NEES (b) Sensor-1 innovation test (c) Sensor-1 confidence interval

FIGURE 8. Performance evaluation of the proposed algorithm for single sensor ECM scenario.

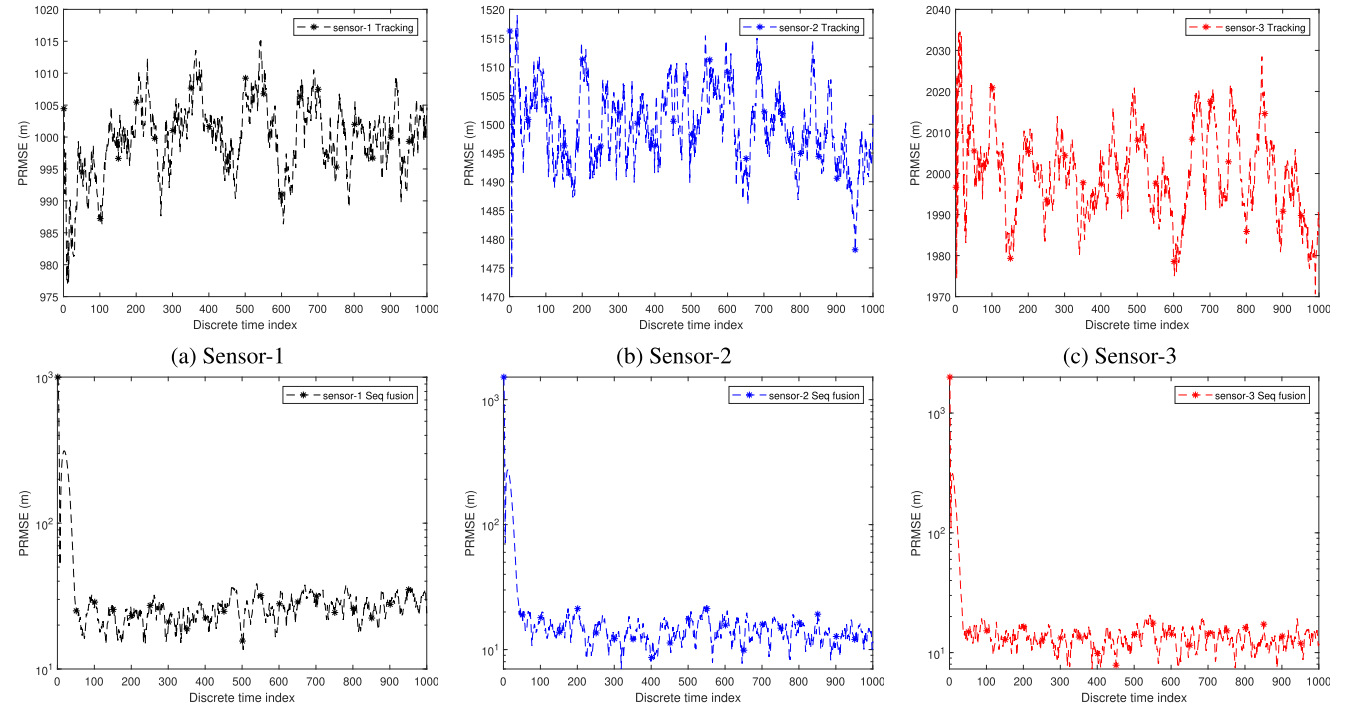

(a) Sensor-1 (b) Sensor-2 (c) Sensor-3

(d) Sensor-1 (e) Sensor-2 (f) Sensor-3

FIGURE 9. (a-c) Tracking performance, (d-f) Sequential fusion performance.

Meaning that, the T2TA model reports that all the tracks are of separate origin, despite all the tracks belonging to the same origin.

2) SEQUENTIAL FUSION PERFORMANCE

Each track is compensated with the estimated range deception parameter Δr_i, and then the sequential fusion is performed. Similar to the single jammer case, the initialization of the fused track is performed by using local tracks. That is, $\mathbf{x}_f(k|k) = \mathbf{x}(k|k)$ and $\mathbf{P}_f(k|k) = \mathbf{P}(k|k)$ at $k = 1$. It can be seen from Figs. 9d-9f that, for all the local tracks fused estimate is equal to the tracking PRMSE of the initial scan at $k = 1$. Similar to the single jammer case, we observed that all the local track's fusion PRMSE decreases over time. This indicates that, the deception parameter compensation followed by sequential fusion brings all the fused tracks together. Since the deception parameter is 1000m for local track-1, 1500m for local track-2, and 2000m for local track-3, the sequential fusion PRMSE starts around the same value and finally reduces to minimum value. Henceforth, one can visualize that the local tracks converges to a single track over time, after performing the deception parameter compensation.

3) DECEPTION PARAMETER EVALUATION

The deception parameter of all the local tracks is estimated, and its corresponding PRMSE is plotted in Fig. 10. Initially, the deception parameter is zero, and hence PRMSE at $k = 1$ is higher and equal to the value of the deception parameter. Along with the estimated deception parameter, we also plotted the $\sqrt{B - CRLB}$, $\sqrt{R - CRLB}$ and $\sqrt{\Sigma}$. Here, we can observe that the estimator is working effectively, and the estimated deception is coming closer to the CRLB value.

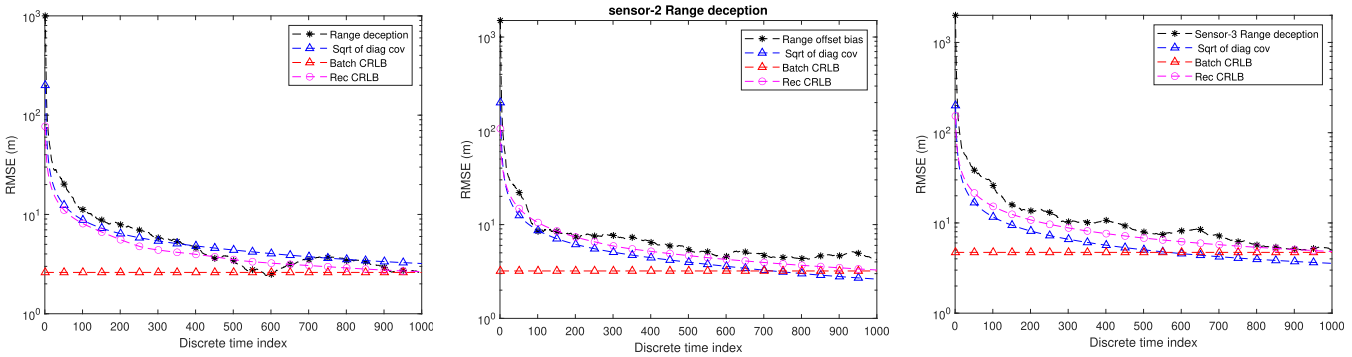

(a) Sensor-1 (b) Sensor-2 (c) Sensor-3

FIGURE 10. Range deception parameters evaluation in multiple jammers.

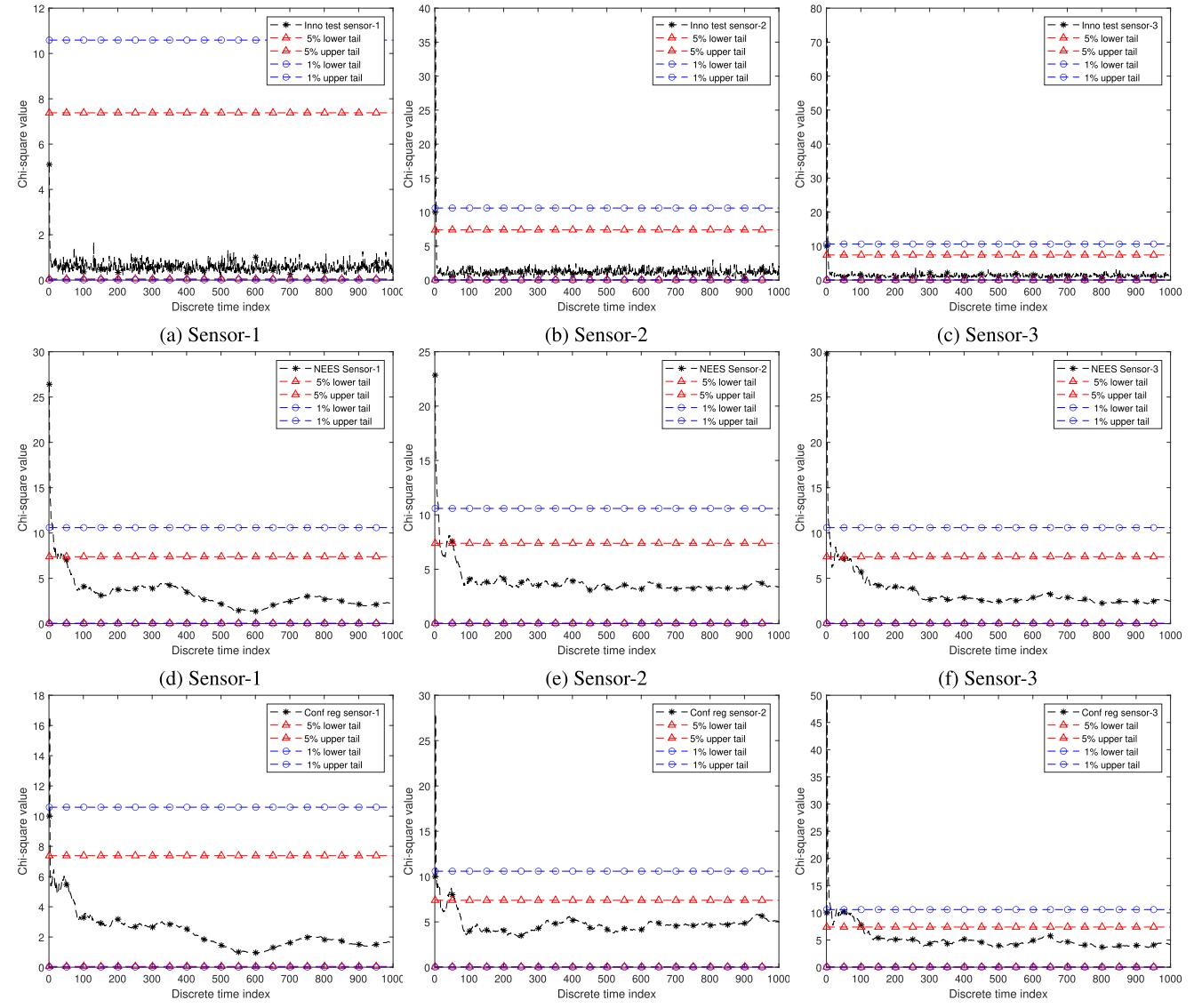

(a) Sensor-1 (b) Sensor-2 (c) Sensor-3

(d) Sensor-1 (e) Sensor-2 (f) Sensor-3

(g) Sensor-1 (h) Sensor-2 (i) Sensor-3

FIGURE 11. (a–c) Innovation test, (d–f) NEES test, and (g–i) Confidence interval for multiple local track ECM scenario.

4) ESTIMATOR PERFORMANCE EVALUATION

To evaluate the performance of the estimator we have considered the similar tests as that of single jammer case. Figs. 11a–11c provides the plots corresponding to the innovation test, whereas Figs. 11d–11f depicts the NEES test, and finally Figs. 11g–11i shows the plots corresponding to

the confidence interval test. From the plots, it is evident that the value of the estimated parameter falls within chi-square distribution of 5% tail probability.

VII. CONCLUSION

This paper presents a deception parameter estimation algorithm for countering RGPO ECM in a networked radar scenario. The RGPO attack is detected, and the range gate deception parameter is estimated for the deceived local track. A track-to-track association is formulated at the fusion node to detect the deceived tracks using all the available local tracks. Once the attack is detected, the weight matrix, pseudo-measurement, pseudo-measurement covariance at the fusion center are recreated by utilizing the tracklet framework (using updated state and updated covariance from the local tracker). Moreover, all the local tracks except deceived track is compensated and sequentially fused to create a reference measurement. The deception parameter of the deceived track is estimated by deploying a recursive least squares framework with the help of the pseudo-measurement and reference measurement. Further, the proposed algorithm was analyzed for single and multiple RGPO ECM scenarios and is validated by using tracker accuracy, fusion accuracy, and estimator accuracy. Besides, the estimated deception parameter is in agreement with the achievable CRLB. Furthermore, the results are quantified with a Position Root Mean Square Error (PRMSE), CRLB, innovation test, NEES test, and confidence interval. In addition, the simulation results demonstrate that, the proposed estimator efficiency is below the 5% tail probability of chi-square distribution. Moreover, it is evident from the results that the proposed technique is efficient for both single and multiple RGPO ECM cases.

The future directions of the work are as follows: 1. In networked radar systems, the radars are able to exchange information from radars and the fusion node. Therefore, once the deception parameter is calculated at the fusion node, that can be sent back to the respective sensor to correct the received measurements in the following scan. 2. In RGPO ECM, traditionally, the tracker reports this effect as a track breakage. Therefore, one can look into the problem of associating the tracks before RGPO ECM and after RGPO ECM to declare the ECM attack. Moreover, the deviation in the tracks can be further utilized to calculate the range deception. 3. In addition, to the range-azimuth measurement, one can consider the signal attributes like received signal amplitude to declare the ECM attack and then associate the tracks over the period of time in an S-D assignment framework to mitigate this effect. 4. Further, this paper considers a single target for simplicity. Whereas, in the multiple target case, the track-to-track association may yield the wrong association. Hence, one should look into the appropriate solution to address this issue.

REFERENCES

[1] Z. Geng, "Evolution of netted radar systems," *IEEE Access*, vol. 8, pp. 124961–124977, 2020.

[2] C. Yang, L. Feng, H. Zhang, S. He, and Z. Shi, "A novel data fusion algorithm to combat false data injection attacks in networked radar systems," *IEEE Trans. Signal Inf. Process. Netw.*, vol. 4, no. 1, pp. 125–136, Mar. 2018.

[3] T. Kirubarajan, Y. Bar-Shalom, W. D. Blair, and G. A. Watson, "IMM-PDAF for radar management and tracking benchmark with ECM," *IEEE Trans. Aerosp. Electron. Syst.*, vol. 34, no. 4, pp. 1115–1134, Oct. 1998.

[4] A. Farina and M. Skolnik, "Electronic counter-countermeasures," in *Radar Handbook*, vol. 2. New York, NY, USA: McGraw-Hill, 2008.

[5] H. Zhou, C. Dong, R. Wu, X. Xu, and Z. Guo, "Feature fusion based on Bayesian decision theory for radar deception jamming recognition," *IEEE Access*, vol. 9, pp. 16296–16304, 2021.

[6] X. Deng, J. Hu, and H. Liu, "Tracking in the presence of RGPO or VGPO using the Kalman filter with a new modified PDA," in *Proc. IET Int. Radar Conf.*, 2013, pp. 1–4.

[7] S. D. Berger, "Digital radio frequency memory linear range gate stealer spectrum," *IEEE Trans. Aerosp. Electron. Syst.*, vol. 39, no. 2, pp. 725–735, Apr. 2003.

[8] F. Bandiera, A. Farina, D. Orlando, and G. Ricci, "Detection algorithms to discriminate between radar targets and ecm signals," *IEEE Trans. Signal Process.*, vol. 58, no. 12, pp. 5984–5993, Dec. 2010.

[9] N. Liu, S.-S. Zhao, and L.-R. Zhang, "A radar ECCM scheme based on full-rate orthogonal pulse block," *J. Comput. Inf. Syst.*, vol. 9, no. 24, pp. 9771–9779, 2013.

[10] C. Huang, Z. Chen, and R. Duan, "Novel discrimination algorithm for deceptive jamming in polarimetric radar," in *Proc. Int. Conf. Inf. Technol. Softw. Eng.* Berlin, Germany: Springer, 2013, pp. 359–365.

[11] M. Greco, F. Gini, and A. Farina, "Combined effect of phase and RGPO delay quantization on jamming signal spectrum," in *Proc. IEEE Int. Radar Conf.*, May 2005, pp. 37–42.

[12] B. Rao, S. Xiao, X. Wang, and T. Wang, "Maximum likelihood approach to the estimation and discrimination of exoatmospheric active phantom tracks using motion features," *IEEE Trans. Aerosp. Electron. Syst.*, vol. 48, no. 1, pp. 794–819, Jan. 2012.

[13] B. Rao, Y.-L. Zhao, S.-P. Xiao, and X.-S. Wang, "Discrimination of exo-atmospheric active decoys using acceleration information," *IET Radar, Sonar Navigat.*, vol. 4, no. 4, pp. 626–638, 2010.

[14] X. Wang, G. Zhang, X. Wang, Q. Song, and F. Wen, "ECCM schemes against deception jamming using OFDM radar with low global PAPR," *Sensors*, vol. 20, no. 7, p. 2071, Apr. 2020. [Online]. Available: https://www.mdpi.com/1424-8220/20/7/2071

[15] W. D. Blair, G. A. Watson, T. Kirubarajan, and Y. Bar-Shalom, "Benchmark for radar allocation and tracking in ECM," *IEEE Trans. Aerosp. Electron. Syst.*, vol. 34, no. 4, pp. 1097–1114, Oct. 1998.

[16] W. D. Blair, G. A. Watson, G. L. Gentry, and S. A. Hoffman, "Benchmark problem for beam pointing control of phased array radar against maneuvering targets in the presence of ECM and false alarms," in *Proc. Amer. Control Conf. (ACC)*, Jun. 1995, pp. 2601–2605.

[17] B. J. Slocumb, P. D. West, T. N. Shirey, and E. W. Kamen, "Tracking a maneuvering target in the presence of false returns and ECM using a variable state dimension Kalman filter," in *Proc. Amer. Control Conf. (ACC)*, vol. 4, Jun. 1995, pp. 2611–2615.

[18] S. S. Blackman, R. J. Dempster, M. T. Busch, and R. F. Popoli, "IMM/MHT solution to radar benchmark tracking problem," *IEEE Trans. Aerosp. Electron. Syst.*, vol. 35, no. 2, pp. 730–738, Apr. 1999.

[19] G. Lu, S. Luo, H. Gu, Y. Li, and B. Tang, "Adaptive biased weight-based RGPO/RGPI ECCM algorithm," in *Proc. IEEE CIE Int. Conf. Radar*, Oct. 2011, pp. 1067–1070.

[20] X. Fu, C. Jiang, Z. Wang, and M. Gao, "Anti-vessel end-guidance radar ECCM against deception jamming of range gate pull off," in *Proc. IET Conf. Publications*, Jan. 2009, p. 82.

[21] W. Xiong, G. Zhang, F. Wen, Y. Zhang, and J. Yin, "Trilinear decomposition-based spatial-polarisational filter method for deception jamming suppression of radar," *IET Radar, Sonar Navigat.*, vol. 10, no. 4, pp. 765–773, Apr. 2016.

[22] S. Zhao and Z. Liu, "Deception parameter estimation and discrimination in distributed multiple-radar architectures," *IEEE Sensors J.*, vol. 17, no. 19, pp. 6322–6330, Oct. 2017.

[23] S. Zhao, L. Zhang, Y. Zhou, N. Liu, and J. Liu, "Discrimination of active false targets in multistatic radar using spatial scattering properties," *IET Radar, Sonar Navigat.* , vol. 10, no. 5, pp. 817–826, 2016.

[24] X. R. Li, B. J. Slocumb, and P. D. West, "Tracking in the presence of range deception ECM and clutter by decomposition and fusion," *Proc. SPIE*, vol. 3809, pp. 198–210, Oct. 1999, doi: 10.1117/12.364050.

[25] B. J. Slocumb, P. D. West, and X. R. Li, "Implementation and analysis of the decomposition-fusion ECCM technique," *Proc. SPIE*, vol. 4048, pp. 486–497, Jul. 2000, doi: 10.1117/12.392001.
[26] K. Davidson and J. Bray, "Understanding digital radio frequency memory performance in countermeasure design," *Appl. Sci.*, vol. 10, no. 12, p. 4123, Jun. 2020.
[27] G. E. J. Du, "DRFM system based on the principle of radar deception," *Int. J. Simul., Syst., Sci. Technol.*, vol. 17, no. 37, pp. 1–17, Jan. 2016.
[28] B. Slocumb and P. West, "ECM modeling for multitarget tracking and data association," *Multitarget-Multisensor Tracking, Appl. Adv.*, vol. 3, pp. 395–458, 2000.
[29] Y. Bar-Shalom, X. R. Li, and T. Kirubarajan, *Estimation With Applications to Tracking and Navigation: Theory Algorithms and Software*. Hoboken, NJ, USA: Wiley, 2004.
[30] M. A. Richards, J. Scheer, W. A. Holm, and W. L. Melvin, "Principles of modern radar," SciTech Publisher, Raleigh, NC, USA, Tech. Rep., 2010.
[31] M. Barbary and P. Zong, "Novel anti-stealth on sub-Nyquist scattering wave deception jammer with stratospheric balloon-borne bistatic radar using KA-STAP-FTRAB algorithm," *IEEE Sensors J.*, vol. 15, no. 11, pp. 6437–6453, Nov. 2015.
[32] Z. Hao and M. Luo, "Adaptive mainlobe jamming suppression method for STAP airborne radar," in *Proc. IET Int. Radar Conf.*, 2013, pp. D0629–D0630.
[33] N. K. Jablon, "Adaptive beamforming with the generalized sidelobe canceller in the presence of array imperfections," *IEEE Trans. Antennas Propag.*, vol. AP-34, no. 8, pp. 996–1012, Aug. 1986.
[34] X. Chen and B. Chen, "Anti-jamming approach based on radar transmitted waveform matching," *EURASIP J. Adv. Signal Process.*, vol. 2021, no. 1, pp. 1–19, Dec. 2021.
[35] W. Yu and W. Chen, "Smart noise jamming suppression technique based on blind source separation," *Int. J. Signal Process. Syst.*, vol. 7, no. 1, pp. 14–19, Mar. 2019.
[36] J. Zhang, X. Zhu, and K. Wang, "A waveform diversity technique for countering RGPO," in *Proc. IET Int. Radar Conf.*, 2009, pp. 1–4.
[37] Y. Lu, M. Li, H. Chen, Z. Wang, and L. Zuo, "Countering DRFM range gate pull-off jamming based on singular spectrum analysis," *J. Electron. Inf. Technol.*, vol. 38, no. 3, pp. 600–606, 2016.
[38] Y. He, X. Wei, X. Hong, W. Shi, and Y. Gong, "Multi-target multi-camera tracking by tracklet-to-target assignment," *IEEE Trans. Image Process.*, vol. 29, pp. 5191–5205, 2020.
[39] R. Popp, K. Pattipati, Y. Bar-Shalom, and R. Gassner, "An adaptive M-best SD assignment algorithm and parallelization for multitarget tracking," in *Proc. IEEE Aerosp. Conf.*, vol. 5, Mar. 1998, pp. 71–84.
[40] L. Zhang, D. Sidoti, A. Bienkowski, K. R. Pattipati, Y. Bar-Shalom, and D. L. Kleinman, "On the identification of noise covariances and adaptive Kalman filtering: A new look at a 50 year-old problem," *IEEE Access*, vol. 8, pp. 59362–59388, 2020.
[41] C. Yang, H. Zhang, F. Qu, and Z. Shi, "Secured measurement fusion scheme against deceptive ECM attack in radar network," *Secur. Commun. Netw.*, vol. 9, no. 16, pp. 3911–3921, Nov. 2016.
[42] B. F. La Scala and A. Farina, "Choosing a track association method," *Inf. Fusion*, vol. 3, no. 2, pp. 119–133, Jun. 2002.
[43] Y. Zhu, S. Zhou, G. Gao, and K. Ji, "Emitter target tracking by tracklet association using affinity propagation," *IEEE Sensors J.*, vol. 15, no. 10, pp. 5645–5653, Oct. 2015.
[44] O. E. Drummond, "Track and tracklet fusion filtering," in *Signal Data Process. Small Targets 2002*, vol. 4728, pp. 176–195, Aug. 2002.
[45] E. Taghavi, R. Tharmarasa, T. Kirubarajan, and Y. Bar-Shalom, "Bias estimation for practical distributed multiradar-multitarget tracking systems," in *Proc. 16th Int. Conf. Inf. Fusion*, 2013, pp. 1304–1311.
[46] X. Sun, S. Zhu, D. Jin, Z. Liang, and G. Xu, "Tracklet association for object tracking," in *Proc. Chin. Control Decis. Conf. (CCDC)*, May 2016, pp. 107–112.
[47] Y. Bar-Shalom, P. K. Willett, and X. Tian, *Tracking Data Fusion*, vol. 11. Storrs, CT, USA: YBS Publishing, 2011.
[48] P. Ivanov, S. Ali-Loytty, and R. Piche, "Evaluating the consistency of estimation," in *Proc. Int. Conf. Localization GNSS (ICL-GNSS)*, Jun. 2014, pp. 1–5.
[49] E. Meir and T. Routtenberg, "Cramér-Rao bound for estimation after model selection and its application to sparse vector estimation," *IEEE Trans. Signal Process.*, vol. 69, pp. 2284–2301, 2021.
[50] H. L. Van Trees and K. L. Bell, *CramerRao Lower Bound for Tracking Multiple Targets*. Hoboken, NJ, USA: Wiley, 2007, pp. 828–833.
[51] F. Govaers, A. Charlish, and W. Koch, "Covariance debiasing for the distributed Kalman filter," Tech. Rep., 2013.
[52] C.-Y. Chi, C.-H. Chen, C.-C. Feng, and C.-Y. Chen, "Fundamentals of statistical signal processing," in *Blind Equalization and System Identification: Batch Processing Algorithms, Performance and Applications*. London, U.K.: Springer, 2006, pp. 83–182.
[53] M. Mallick and B. L. Scala, "Comparison of single-point and two-point difference track initiation algorithms using position measurements," *Acta Autom. Sinica*, vol. 34, no. 3, pp. 258–265, 2008.

PURUSHOTTAMA LINGADEVARU (Member, IEEE) received the B.E. degree in electronics and communication engineering and the M.Tech. degree in electronics from Visvesvaraya Technological University (VTU), Belagavi, Karnataka, India, in 2005 and 2007, respectively. He is currently pursuing the Ph.D. degree with the National Institute of Technology Karnataka (NIT-K), Surathkal, India. He has been working as an Assistant Professor with the Department of Electronics and Communication Engineering, Siddaganga Institute of Technology, Tumkur, Karnataka, since 2013. He was deputed to pursue the Ph.D. degree from NIT-K, in 2018. His research interests include passive radars, cognitive radio, and target tracking.

BETHI PARDHASARADHI (Member, IEEE) received the B.Tech. degree in electronics and communication engineering from Jawaharlal Nehru Technological University, Kakinada (JNTU-K), Andhra Pradesh, India, in 2014, and the M.Tech. degree in VLSI design from the Indian Institute of Information Technology and Management, Gwalior (IIITM), Madhya Pradesh, India, in 2016. He is currently pursuing the Ph.D. degree with the National Institute of Technology Karnataka (NIT-K), Surathkal, India. He was a receipientt of the Sir C. V. Raman Award from the Institution of Engineering and Technology (IET) for outstanding academics and research. He was a Visiting Ph.D. Scholar with the ETF Laboratory, McMaster University, Canada, under the supervision of Prof. T. Kirubarajan, from 2018 to 2019. His research interests include intentional interference in navigation, target tracking, and information fusion.

PATHIPATI SRIHARI (Senior Member, IEEE) received the B.Tech. degree in electronics and communication engineering from Sri Venkateswara University, the master's degree in communications engineering and signal processing from the University of Plymouth, U.K., and the Ph.D. degree in the field of radar signal processing from Andhra University, in 2012. He is currently working as an Assistant Professor with the National Institute of Technology Karnataka, Surathkal, India. He worked as a Visiting Assistant Professor with McMaster University, Canada, in 2014. He received the 2010 IEEE Asia Pacific Outstanding Branch Counselor Award. He is a Senior Member of ACM. He is a fellow of IETE and a member of IEICE, Japan. He received Young Scientist Award from the Department of Science and Technology (DST), New Delhi, to carry out sponsored research project titled development of efficient target tracking algorithms in the presence of ECM. His research interests include radar target tracking, radar waveform design, and efficient DSP algorithms for radar applications.